Design and fabrication of a low head vertical axis turbine for power generation in water pipelines
(Micro Hydro Turbine)

By

Syed Osama bin Ahsan	NUST201200442BSMME11112F
Omer Farid	NUST201200801BSMME11112F
Muhammad Talha Naeem Rao	NUST201201198BSMME11112F
Ali Altaf	NUST201200390BSMME11112F

Supervised By

Assistant Professor Ammar Tariq

School of Mechanical and Manufacturing Engineering,

National University of Sciences and Technology (NUST),

Islamabad, Pakistan

June, 2016

National University of Sciences & Technology

FINAL YEAR PROJECT REPORT

We hereby recommend that the dissertation prepared under our supervision by:

Syed Osama bin Ahsan	Reg # NUST201200442BSMME11112F
Omer Farid	Reg # NUST201200801BSMME11112F
Muhammad Talha Naeem Rao	Reg #NUST201201198BSMME11112F
Ali Altaf	Reg # NUST201200390BSMME11112F

Titled: **Design and fabrication of a low head vertical axis turbine for power generation in water pipelines (Micro Hydro Turbine)** be accepted in partial fulfillment of the requirements for the award of Bachelors of Engineering in Mechanical Engineering degree with (_____ grade)

English and format checked by Ms Aamna Hassan, Signature:__________________

Guidance Committee Members

1. Name: ______________________________ Signature:_________________

2. Name: ______________________________ Signature:_________________

3. Name: ______________________________ Signature:_________________

Supervisor's Name: ________________________ Signature:_________________

Date:__________________

_____________________ Head of Department

____________________ Date

COUNTERSIGNED

Date:_______________

____________________ Dean/Principal

Declaration

I/We certify that this research work titled "***Design and fabrication of a low head vertical axis turbine for power generation in water pipelines***" is my own work. The work has not been presented elsewhere for assessment. The material that has been used from other sources it has been properly acknowledged / referred.

Syed Osama bin Ahsan

NUST201200442BSMME11112F

Omer Farid

NUST201200801BSMME11112F

Muhammad Talha Naeem Rao

NUST201201198BSMME11112F

Ali Altaf

NUST201200390BSMME11112F

Copyright Statement

Dedicated to my parents

Acknowledgments

First of all I would thank ALLAH Almighty, who gave me knowledge and dedication to be able to complete this research. I would also like to thanks our Faculty advisor who, at each and every step, assisted, encouraged and guided us to complete the project successfully. I would like to thank Dr. Aamir Mubashir as well for his invaluable guidance regarding FEM analysis which was a major part of our project.

I would also show my gratitude to our Senior Mr. Ammar Naseem for his guidance in ANSYS simulation and in understanding of the basics of hydro turbines. Alongside others, special thanks to Mr. Safeer for his help in testing phase of our project.

Abstract

Our team started this project with the objective of designing a power generation system that could be installed inside municipal water pipes. The purpose was to understand and find out if setting up such a system in gravity driven water pipes will actually yield results or not. The idea was to set up small capacity power generation system, hence the name micro-hydro turbine and to discover new way of providing electricity to the people. To design such a system, we studied different types of turbines and discovered that vertical axis turbines were most suited for small capacity generation systems. Working from there, we fabricated a globe shaped, spherical helical turbine that could fit well into any pipe and produce maximum amount of electricity.

To test the feasibility of the design, we took help of several different software and simulated the system testing the power output, forces application, material strength and fluid interaction with the blades of the turbine. To verify those results, a small prototype was fabricated which was then tested in a small canal. The results, though not exactly perfect, were still close to the theoretical calculations which was evidence enough to substantiate the claim that the design was feasible enough and for larger diameter pipes, it would be an ideal turbine to be installed in a pipe.

Table of Contents

List of Figures

List of Tables

Symbols

Symbol	Description	Unit
α	Angle of Attack	$[^\circ]$
γ	Pitching Angle	$[^\circ]$
μ	Dynamic Viscosity	$\left[\frac{\mathrm{kg}}{\mathrm{m \cdot s}}\right]$
ω	Angular Velocity	$\left[\frac{\mathrm{rad}}{\mathrm{s}}\right]$
ρ	Density	$\left[\frac{\mathrm{kg}}{\mathrm{m}^3}\right]$
θ	Azimuthal Angle	$[^\circ]$
a	Interference Factor	$[-]$
A	Area	$[\mathrm{m}^2]$
B	Number of Blades	$[-]$
c	Chord	[m]
C_D	Drag Coefficient	$[-]$
C_L	Lift Coefficient	$[-]$
C_P	Power Coefficient	$[-]$
D	Diameter	[m]
F_D	Drag Force	[N]
F_L	Lift Force	[N]
F_N	Normal Force	[N]
F_T	Tangential Force	[N]
h	Height	[m]
L	Length	[m]
P	Power	[W]
p	Pressure	[Pa]
Q	Torque	[Nm]
R	Radius	[m]
Re	Reynolds Number	$[\cdot]$

Chapter 1

Introduction

1.1 Background:

Micro hydro is a type of hydroelectric power that typically produces from 5 kW to 100 kW of electricity using the natural flow of water. Installations below 5 kW are called Pico hydro. These installations can provide power to an isolated home or small community, or are sometimes connected to electric power networks, particularly where net metering is offered. There are many of these installations around the world, particularly in developing nations as they can provide an economical source of energy without the purchase of fuel. Micro hydro systems complement solar PV power systems because in many areas, water flow, and thus available hydro power, is highest in the winter when solar energy is at a minimum. Micro hydro is frequently accomplished with a Pelton for high head, low flow water supply. The installation is often just a small dammed pool, at the top of a waterfall, with several hundred feet of pipe leading to a small generator housing.

1.2 Aims and Objectives:

The small VAWT has the possibility to be installed in municipal pipes for power generation where water is gravity driven. It is interesting to investigate how a VAWT can be optimized to have a higher power coefficient. This project decided to focus on the helical spherical turbine because of its globe shaped construction that could be fit in covering the best part of the pipe.

The main objective was to **Design and fabricate a low head vertical axis turbine for power generation in water pipelines**. The design of the turbine will be kept such that it creates minimum pressure drop and yet is able to produce electricity that is sufficient compared to the cost input.

It will be investigated how the power output depends on the number of blades and different wing profiles.

The main questions that will be addressed are:

- Will increasing the curvature (camber) of the wing profile affect the performance of a turbine?
- Will Increase in the number of blades increase the power output of the turbine?
- Will the results from the prototype tested match the results from the computer model?

1.3 Research Methodology:

While designing the turbine, the first stage was to understand the core concepts of turbine design and the mathematical model that determines the performance outputs of the turbine by thoroughly studying the literature present on the turbines and decide the most suited type of turbine available for the project. After selecting the type, the team investigated the different design parameters of the turbine as to how their change affected the outcome and chose the best option to our understanding.

1.4 Thesis Structure:

Following are the fundamental chapters which will be encompassed in this thesis.

- **Chapter 2: Literature Review:**

  This chapter explains the methodology employed for conducting literature review, stages at which it was conducted, basic learning outcomes of the literature review and ideas taken from different available researches.

  - **The general literature review of turbine is discussed in this chapter. However, particular aspect such as literature review regarding mathematical modelling is presented in chapter 3.**

- **Chapter 3: Mathematical & Solid Modelling:**

  This chapter will give a brief overview of all the mathematical equations derived during the design of the micro hydro turbine. Modelling and simulations from QBlade and ANSYS are included as well for both original turbine as well as the prototype. Also, the analytical results are presented in this chapter for both turbines.

- **Chapter 4: Analysis (FEM):**

  All the stress analysis conducted after solid designing performed will be described here in this chapter in detail done on the prototype as well as the material selection process and the reasons for doing so.

- **Chapter 5: Fabrication & Testing:**

  This chapter encompasses all the activities performed during the fabrication of the turbine and the subsequent testing of it. The results of the testing are also explained in this chapter.

- **Chapter 6: Conclusion and Recommendations:**

  The conclusions drawn from the testing results are compared with the simulation results and recommendations are made so as to improve the performance of turbine.

Note:

Our team visited CDA (Capital Development Authority) Islamabad and learned that Simli Dam has a 36’’ diameter pipe that connects the dam with the filtration plant 0.5 km away. The water velocity was 3m/s which makes it a very suitable place to set up our turbine.

The following chapters including designing and simulation of the ‘Original Turbine-proposed to be designed for Simli Dam pipelines-’, as well as those of the prototype alongside it.

Chapter 2

Literature Review

2.1 Need for Micro Hydro Turbine:

Pakistan has abundant supply of free streams and rivers on the northern side of the country. The remoteness of the area and the provision of the electricity to these areas adds huge costs. For the scattered and isolated villagers of the mountainous regions of Pakistan, those costs can be measured not only by low incomes, but by poor health and safety as pinewood sticks and costly kerosene lamps make a precarious substitute for the lack of electricity. These free streams can supply water to the nearby areas through water pipelines.

However, the pipes carrying water are still used just to supply water to nearby homes. The idea of this project is to understand the feasibility of the application of turbine installation within these pipes and whether they are able to sufficiently supply electricity to the nearby residents. The need for provision of electricity is paramount for the development of those regions and micro hydro turbines that can be installed easily because of their relatively smaller size as well of low costs makes it a good alternate source of electricity.

2.2 Wind Turbine and Types:

Wind turbine converts the wind energy into mechanical energy and that mechanical energy is used for the production of electricity. There are two types of primary wind turbine; they are horizontal-axis water turbine (HAWT) and vertical-axis water turbine (VAWT), both of which boast of being better than the other.

HAWTs include both upwind and downwind configuration with various performance enhancers such as diffusers and concentrators. HAWT is more popular because they have better efficiency, but only suitable for places with high wind speed. In contrast, VAWT works well in places with relatively lower strength, but constant wind. The blades are not needed to orient in wind direction as it can work always in the same direction though wind comes from any direction.

Due to better aerodynamic behavior and more efficient in the large scale, HAWT was the popular choice of the researchers. But several factors are turning the head of researchers towards the field of VAWT. They are, VAWT may be more appropriate than HAWT in small scale. VAWTs are suitable for electricity generation in the conditions where traditional HAWTs are unable to give reasonable efficiencies such as low wind velocities and turbulent wind flows. VAWT can operate without any dependence on wind direction. The quiet behavior is more attractive for highly populated places. The cost of complex structure of HAWT blades is higher than simpler VAWT blades. Because of the stalling behavior it can withstand gust wind, which makes it much safer during those weather conditions. This type of rotor can be installed in remote places, away from the main distribution lines and places where large wind farms cannot be installed due to environmental concerns.

Having considered the above mentioned comparison of the two types of turbines, since the aim of our project was to design a small turbine with small power generation, vertical axis turbine was selected.

Then next step was to choose the right type of vertical axis turbine for micro-hydro turbine for which the details of several different types are discussed below.

2.3 Types of Vertical Axis Wind Turbines:

A wide variety of VAWTs have been constructed over the last few decades. They are classified based on aerodynamic and mechanical properties, shape of the blades, and shape of the rotor. The VAWT can be divided into three basic types: Savonius, Darrius and Gorlov Helical Turbine.

2.3.1 Savonius Turbine:

The Savonius turbine uses a rotor made from two or more half-cylinders held together by a disc at each end of the rotor shaft (see figure 2.1). This wind turbine has been popular with both professional and amateur wind turbine developers over the years, because of its simple and robust construction. Unfortunately the Savonius uses drag to extract energy from the wind instead of lift. This means that it cannot, spin faster than the wind so its maximum TSR is one.

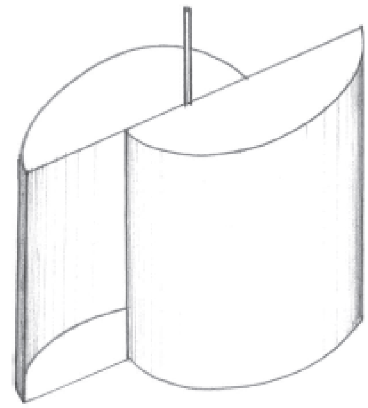

Figure 2.1 Savonius Turbine

2.3.2 Darrius Turbine:

The Darrius turbine is a VAWT with curved blades, which use lift forces generated by the wind hitting airfoils, to create rotation. An example of a Darrius turbine can be seen in figure 2.2. The Darrius turbine can rotate at several times the speed of the wind because its power is generated by lift. Therefore it has a greater TSR than a Savonius, and generally a higher power coefficient.

A disadvantage of the Darrius turbine is that it needs a power source to start rotating because it demands a large torque to overcome its inertia. At the low wind speeds the angle of attack (AOA) is often large, so the blades are in stall thereby creating low or negative torque.

Figure 2.2 Darrius Turbine

2.3.3 Gorlov Helical Turbine:

Gorlov turbine, as shown in Figure 2.3, is a Helical Darrius-type turbine that incorporates both sweep and twist of the blades along an imaginary, cylindrical radius. The Gorlov is considered a cross-flow turbine due to the orientation of the blades.

Its helical design maintains that at some point along the blade's length, the ideal angle of attack is achieved for rotations. This achieves less pulsatory torque problems for a "smoother" drive. As well, for the same reasons, vibrations are mitigated which can lower maintenance and reliability problems.

With these properties in mind, the turbine can be used in any orientation in a flow that is normal to the shaft. This property increases its application potential – It can be mounted and working horizontally, vertically, or angled, assuming a low head application.

Little information is available regarding free-steam, micro-hydro applications for power generation but its potential exists. A river application is considered unique as the majority of applications are focused on very large-scale ocean currents or tidal movements.

Figure 2.3 Gorlov Helical Turbine

Note: Although, these turbines, initially were used as wind turbines, they can and are used as water turbines as well. However, by convention they are still known as wind turbines.

2.4 Aerodynamics of Wind Turbines:

In order to properly analyze the computer model and the prototype of the VAWT, it is necessary to understand the fundamental theories of aerodynamics and how they relate to the concepts of lift and drag. Figure 3.1 shows important terms which will be used throughout the remainder of the report. The terms are Lift (FL), Drag (FD), Normal Force (FN), and Tangential Force (FT). It also displays three key terms for defining those forces; chord (c), relative velocity (W) and angle of attack (AOA,α).

2.4.1 General Lift and Drag Forces:

Lift force is caused by pressure and viscous effects from the air that are exerted on an airfoil [Cengel et al., 2010]. It acts orthogonally to the relative velocity and is oriented perpendicular to the drag force. The air exerts a force on the airfoil in the direction of the flow called drag, which is caused by pressure and friction. The normal and tangential forces are found by summing the tangential and normal components of the lift and drag forces. The AOA is defined as being the angle between the relative velocity and the chord, shown in figure 2.4. The chord is the straight line from the leading edge to the trailing edge of the wing profile.

For objects which are designed to generate lift, the contribution from the viscous effect can be neglected, so the lift force is only depending on the pressure differences at the airfoil's surfaces. The drag force is a sum of friction (skin) drag and pressure (form) drag. The induced drag which is related to end effects of airfoils will be described separately. Both lift and drag coefficients are dependent the airfoil's orientation in the flow.
This orientation is represented by the AOA. Airfoils are designed to generate lift and minimize drag.

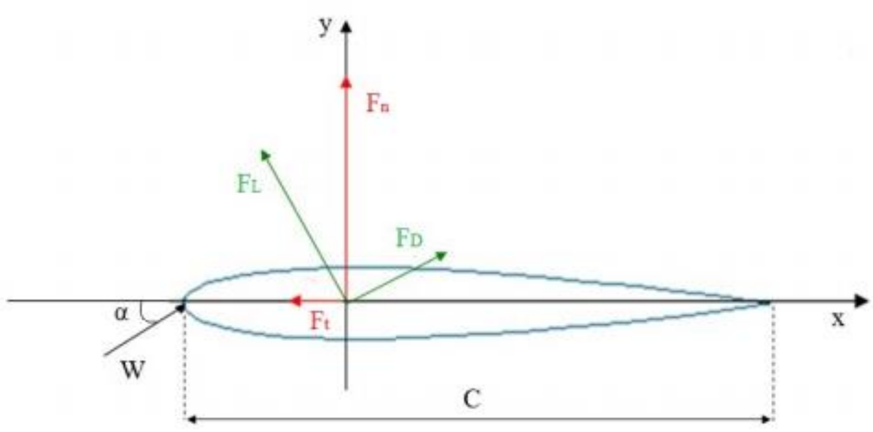

Figure 2.4 Illustration of various terms used in airfoil theory

2.4.2 Lift Force:

Lift is mainly generated by the pressure distribution on the surface of an airfoil. This pressure distribution is formed by the shape of the airfoil. The airfoil is designed so that the top and bottom surfaces can have different curvatures, which means that the flow moving over and under the airfoil will have to take a different length path. For a symmetrical profile, this difference is created by changing the AOA.

Conservation of mass requires that the amount of air before and after the airfoil must remain constant. The difference in path length causes the flow over the longer section (the top surface) to briefly accelerate. According to Bernoulli's equation this increase in velocity results in a decrease in pressure. The pressure vacuum along the top surface of the airfoil creates a pressure gradient which is what creates the lift force. The pressure distribution on an airfoil can be seen in figure 2.5.

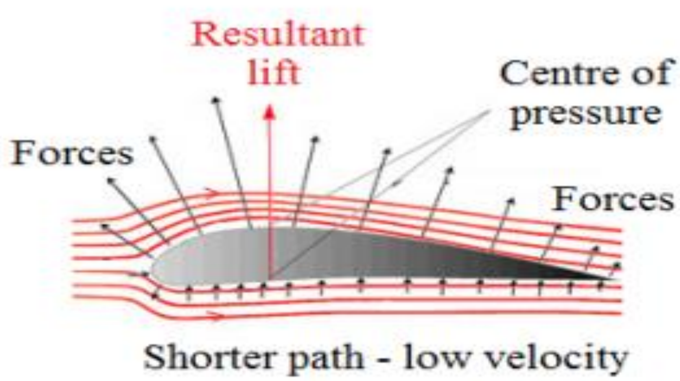

Figure 2.5 Flow across a wing profile and the resulting pressure distribution.

As the flow passes over the airfoil the faster moving fluid on the top must begin to decelerate as it approaches the trailing edge. The flow at the trailing edge must have the same velocity on the top and the bottom of the airfoil. If it does not then there will be a shearing in the flow that will cause significant amount of drag and turbulence downstream of the airfoil. If the flow does have the same velocity on top and bottom of the profile and the trailing edge is sharp, then the Kutta Condition will be met.

This will result in a stagnation point at the trailing edge which allows the air to be smoothly shed from the airfoil. Figure 2.6 shows how there initially is a large pressure drop on the top surface due to the acceleration of the flow, but as the flow passes over the profile the pressure drop decreases so that the velocities on both surfaces of the trailing edge are equal.

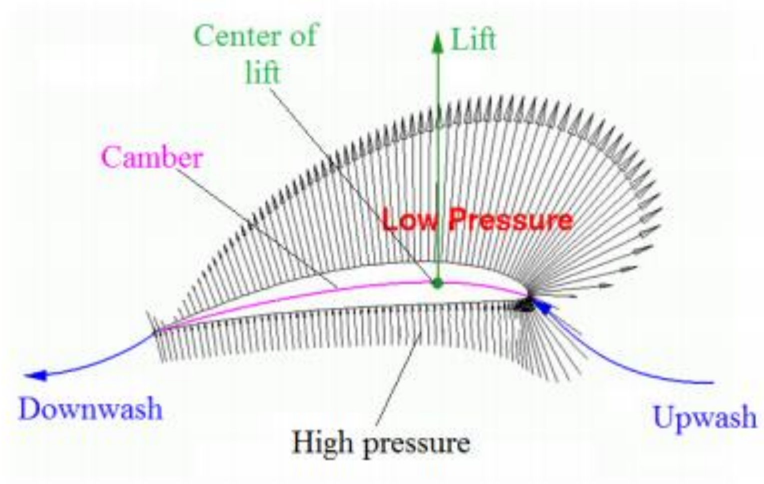

Figure 2.6 Pressure distribution over a wing.

$$C_L = \frac{F_L}{\frac{1}{2} \cdot \rho \cdot V^2 \cdot A}$$

where,

C_L = lift coefficient [-]

F_L = lift force [N]

ρ = density for the fluid $\left[\frac{kg}{m^3}\right]$

V = velocity of the fluid $\left[\frac{m}{s}\right]$

A = area of the airfoil $[m^2]$

The lift coefficient is a non-dimensional number that describes how effectively an airfoil changes the flow to generate lift. Due to the different geometries of airfoils, there are unique values of the coefficients of lift for each airfoil. These lift coefficients is plotted based on AOA at a given Reynolds number.

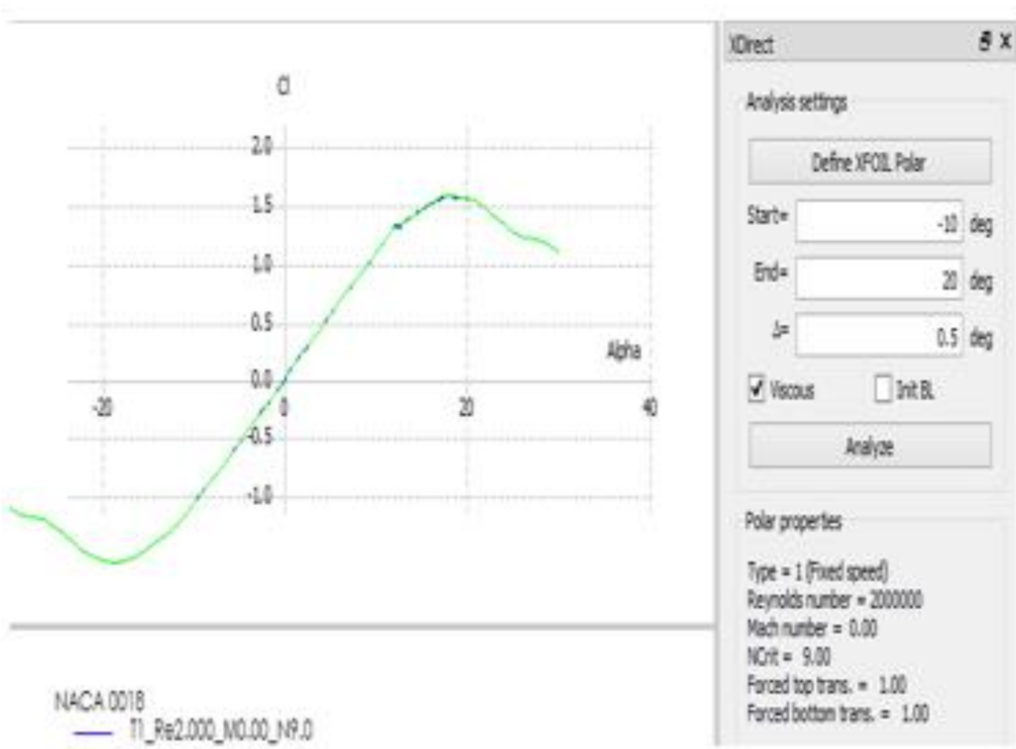

Figure 2.7 Lift curve for NACA 0018 @ Re= 2.0 E6.

When changing the AOA, the velocity and pressure distributions over and under the wing profile will change, which results in different values of lift, shown in figure 3.4. The figure shows that lift will increase linearly with AOA until a point called the stall point. The decrease in the lift coefficient at the stall point is due to a flow separation, where the flow separates prematurely from the airfoil. When the flow separates from the airfoil, the pressure difference between the top and bottom will not be maintained, and there will be no more lift generated at that location and all locations behind it. The AOA which generates a separation point close enough to the leading edge that the lift force decreases is called the critical angle of attack. Any AOA greater than this will cause the wing to be in stall.

2.4.3 Drag force:

Drag forces resist the forward motion of an object, so for vehicles such as airplanes the drag force must be compensated by an increase in thrust. Drag is broken into two categories: friction (skin) drag and pressure (form) drag. Frictional drag is due to surface shear stresses and is a function of viscosity. The Reynolds number is inversely proportional to viscosity, so at higher Reynolds numbers the contribution from frictional drag will become less significant. When frictional drag is exerted on a body in a turbulent flow it is also a function of the surface roughness. A smooth and nonporous material has less frictional drag than a rough or porous one.

The pressure drag is a function of the frontal area and the pressure difference between the front and back of an object. The pressure drag is small for streamlined objects such as an airfoil. When it is not possible for the flow to follow the surface, it separates from a location called the separation point. The flow after the separation point can be described as highly turbulent and creates eddies that are in a low pressure region. This means that the pressure drag will continue to increase as the AOA increases because the pressure gradient from leading to trailing edge is increasing.

Drag is calculated with an equation very similar to lift. Like lift, a non-dimensional number, called the coefficient of drag, has been created to express the drag as a function of AOA and Reynolds number.

$$C_D = \frac{F_D}{\frac{1}{2} \cdot \rho \cdot V^2 \cdot A}$$

where,
C_D = drag coefficient [-]
F_D = drag force [N]
ρ = density for the air $\left[\frac{kg}{m^3}\right]$
V = the velocity of the fluid $\left[\frac{m}{s}\right]$
A = the area of the airfoil $[m^2]$

Considering finite wings, the end effect of the wings will be an important parameter, because there will be a fluid leakage between the top and bottom of the airfoil. The leakage on a lift producing wing, is caused by the flow curling from the high pressure side, to the low pressure side, which is illustrated in figure 2.8.

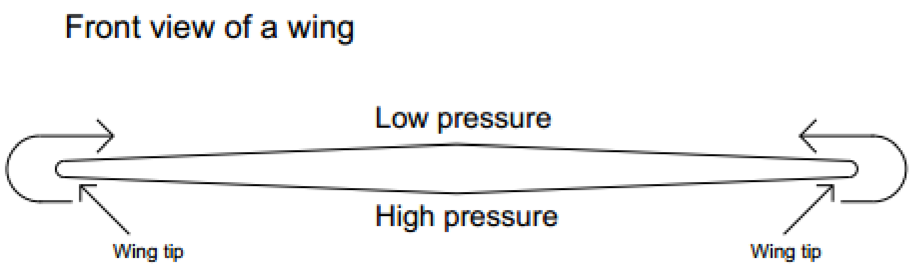

Figure 2.8 Air flow from the bottom to the top around the wing tip.

The curling of flow around the wing tips creates trailing vortex at both wing tips, see figure 2.9. These tip vortices tend to take the surrounding air with them, which creates a small downwards velocity also called downwash.

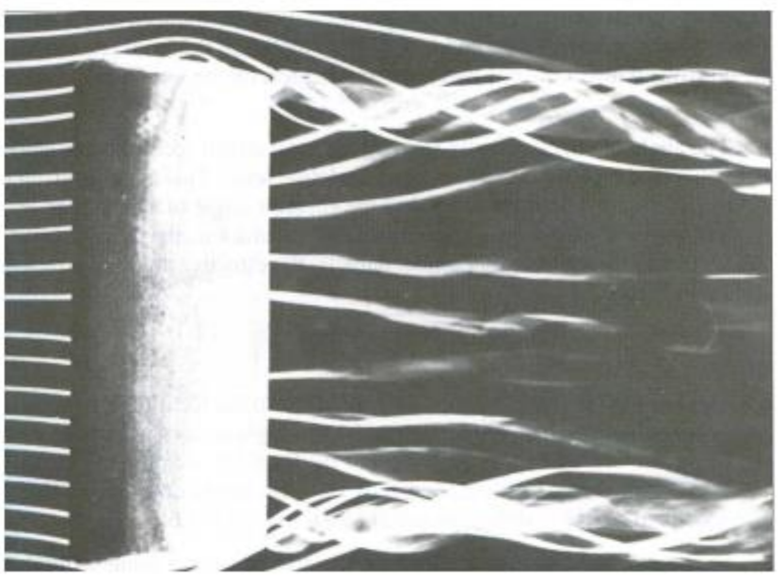

Figure 2.9. Wing profile with wing tip vortices.

This downwash combined with the free stream velocity creates a local relative velocity which reduces the AOA and creates induced drag [Anderson, 2007]. Induced drag is also called the drag due to lift, because the induced drag coefficient is proportional to the lift coefficient squared.

$$C_{D,i} = K \cdot C_L^2$$

where,
$C_{D,i}$ = induced drag coefficient [-]
K = proportional factor

The induced drag is created by the wingtip vortices which are created by the same pressure difference that generates lift. Whenever there are wings of finite length, induced drag is by-product of generating lift force. This is one of the reasons why there is not one ultimate wing profile that maximizes lift and minimizes drag. A profile with maximum lift will also have maximum induced drag.

2.5 Application of Aerodynamics in Vertical Axis Wind Turbines:

VAWTs add a new level of complexity when calculating lift and drag because the relative velocity and AOA are constantly changing. This is because the azimuthal angle (θ), or position of the turbine blades (wing profiles) as the turbine rotates, is always changing. The relationships between the azimuthal angle, relative velocity, and the lift and drag forces is shown in figure 2.10.

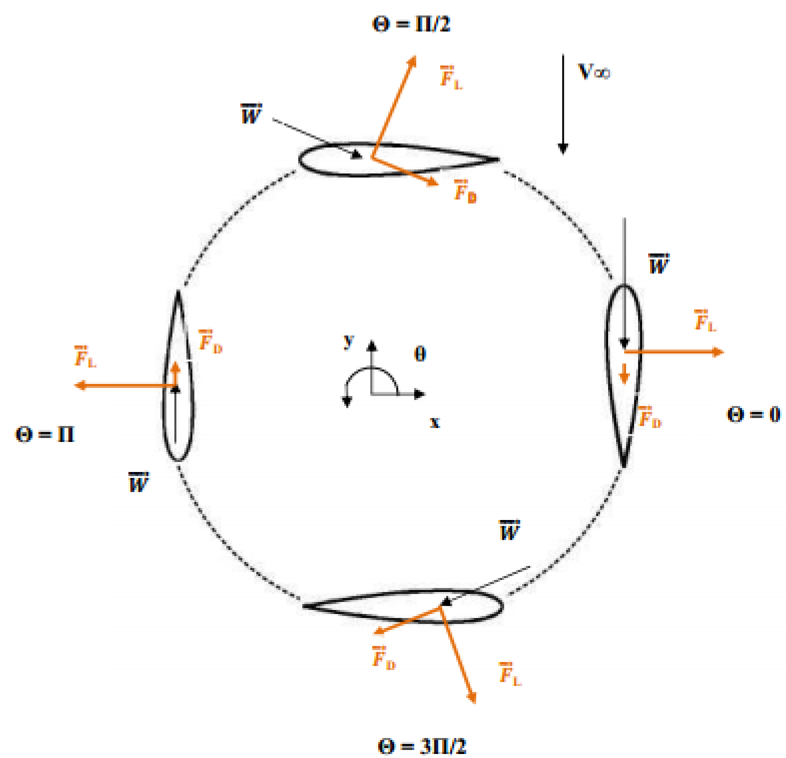

Figure 2.10 Relative velocity and the forces acting on one blade during one revolution

The azimuthal angle dictates the values of the relative velocity and AOA which means lift and drag are a function of the azimuthal angle. In order to optimize the power output of a VAWT, the airfoil design and orientation must be optimized so that the maximum range of azimuthal angles is generating non-stall lift. Additionally the airfoils must be chosen to have minimal drag for the majority of azimuthal angles.

Chapter 3:
Mathematical & Solid Modelling:

Having analyzed the basic air foil design parameters and definitions, the design of Blade Profile and turbine designing is discussed.

Design considerations involve assessing several parameters of blade design to find the most optimum design of blade. To accomplish the task, Blade design software QBlade and Fluid Module of ANSYS were used.

3.1 Defining Parameters for Turbine Design:

1- Diameter of a pipe
2- Velocity of Water
3- Turbine Diameter
4- Turbine Height
5- Blade Air Foil
6- Solidity - Chord Length
7- Number of Blades

In finding a suitable place for the installation of the turbine, we visited CDC Islamabad and learned that Simli Dam has a long 36” Diameter pipe that connects the dam with a filtration plant 0.5 km away. The velocity of the water flowing within it was calculated to be 3m/s. The diameter of the pipe and the velocity of the water, hence, became the determining factors for turbine design.

Since the turbine is globe shaped, the diameter and the height of the turbine are equal. For maximum utilization of the water head, 34’’ diameter turbine was selected to be designed as well as the height of it.

3.1.1 Blade Profile:

The NACA profile is a standard that describes the geometry of an airfoil. NACA profiles can be described by four, five, or six digits, but in this report only the four digit series will be used. Many of the common four digit NACA profiles have experimental data available that gives plots of the coefficients of lift and drag. For uncommon profiles there are programs available to calculate the coefficients of lift and drag.

The NACA profile is shown in figure 3.11, with the terms related to an airfoil. The chord is the straight line, from the leading edge to the trailing edge of the wing profile, see figure 3.1. The mean camber line is a line of points, half way between the lower and upper surfaces. The camber is the difference between the chord and the mean camber line. If the camber of a wing profile is great enough, the chord will travel outside of the physical structure of the wing profile. The mean camber line will always remain inside the wing profile. The thickness is the distance between the upper and lower surfaces oriented normal to the chord.

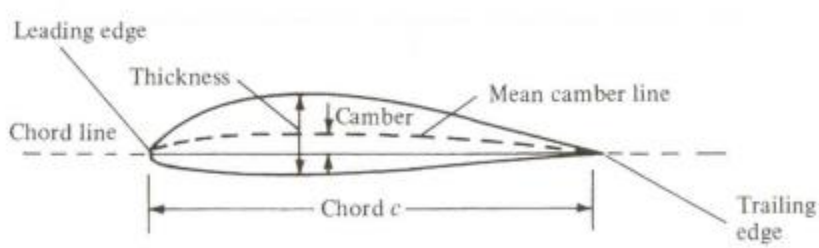

Figure 3.1 Terms used for NACA profiles.

Each digit represents information used for drawing the NACA profile. The functions of each digit in the four digit NACA profiles are described below:

- **1st:** The first digit describes the maximum camber as a percentage of the chord.
- **2nd:** The second digit is the location of the maximum camber, from the leading edge in tenths of the chord.
- **3rd and 4th:** The last two digits describe the maximum thickness in hundredths of chord.

Several blades profiles were analyzed on the software (figure 3.2) and the best one with the highest Cl/Cd ratio was selected. NACA 4415 was selected not only on the basis of the aforementioned ratio, but also the fact that cambered profile is better than symmetrical profiles for self-starting purposes which is a major issue with vertical axis turbines.

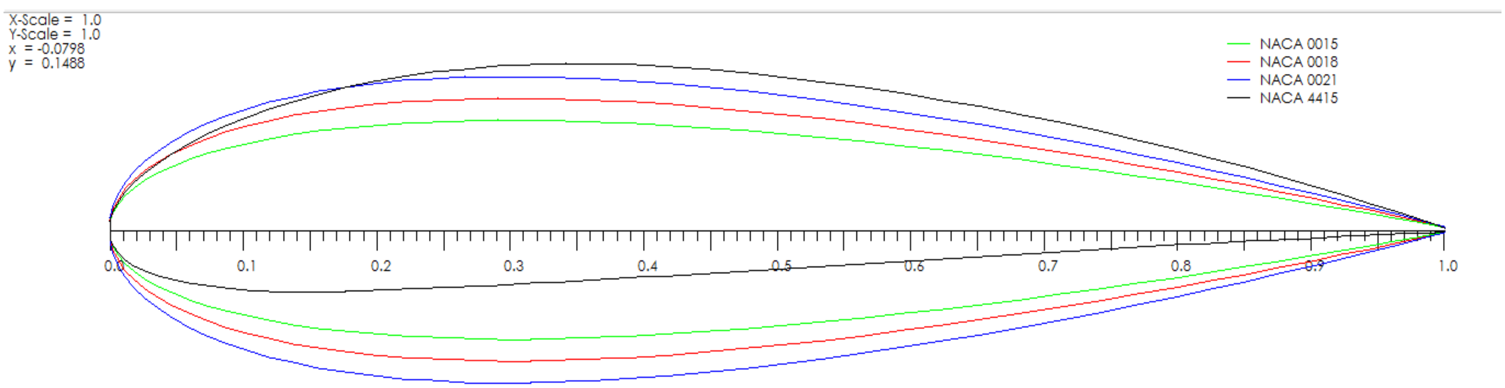

AFoil

	Name	Thickness (%)	at (%)	Camber (%)	at (%)	Points	TE Flap (deg)	TE XHinge	TE YHinge	Show	Points	Centerline	Style
1	Spline foil	9.03	31.20	-0.00	55.10	60	0.00	0.00	0.00	☐	☐	☐	
2	NACA 0015	15.00	29.10	-0.00	21.20	99	0.00	0.00	0.00	☑	☐	☐	
3	NACA 0018	18.00	29.10	0.00	28.50	99	0.00	0.00	0.00	☑	☐	☐	
4	NACA 0021	21.00	29.10	0.00	12.00	99	0.00	0.00	0.00	☑	☐	☐	
5	NACA 4415	15.00	29.10	4.00	39.50	99	0.00	0.00	0.00	☑	☐	☐	

Figure 3.2 NACA profiles under consideration.

3.1.2 C_l/C_d Graph:

Cl = lift Coefficient

Cd = Drag Coefficient

Since the spherical turbine is a lift based turbine, maximizing the lift and minimizing the drag are the main aims to achieve while selecting a profile. The graphs for each blade profile was checked and the best one was thus chosen. As can be seen from the graph, for most of the part along entire 360˚ azimuth angle, the Yellow Line indicating Cl/Cd ratio for NACA 4415 remained above the rest giving a better ratio than others. The fact that it has better self starting performance-meaning it required no initial torque to start- it will still be a more popular choice for the design even it were not the best cl/cd ratio as can be seen in figure 3.4.

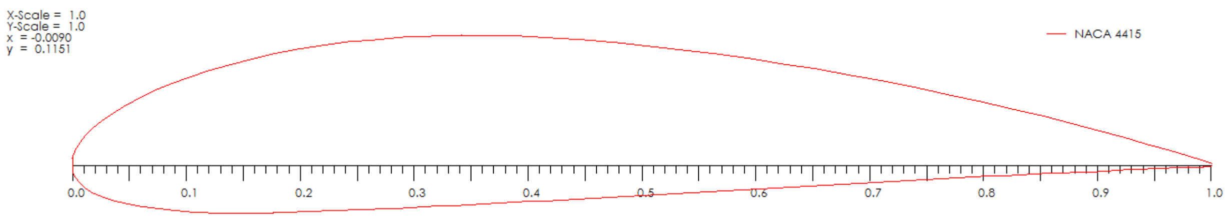

Figure 3.3 NACA 4415.

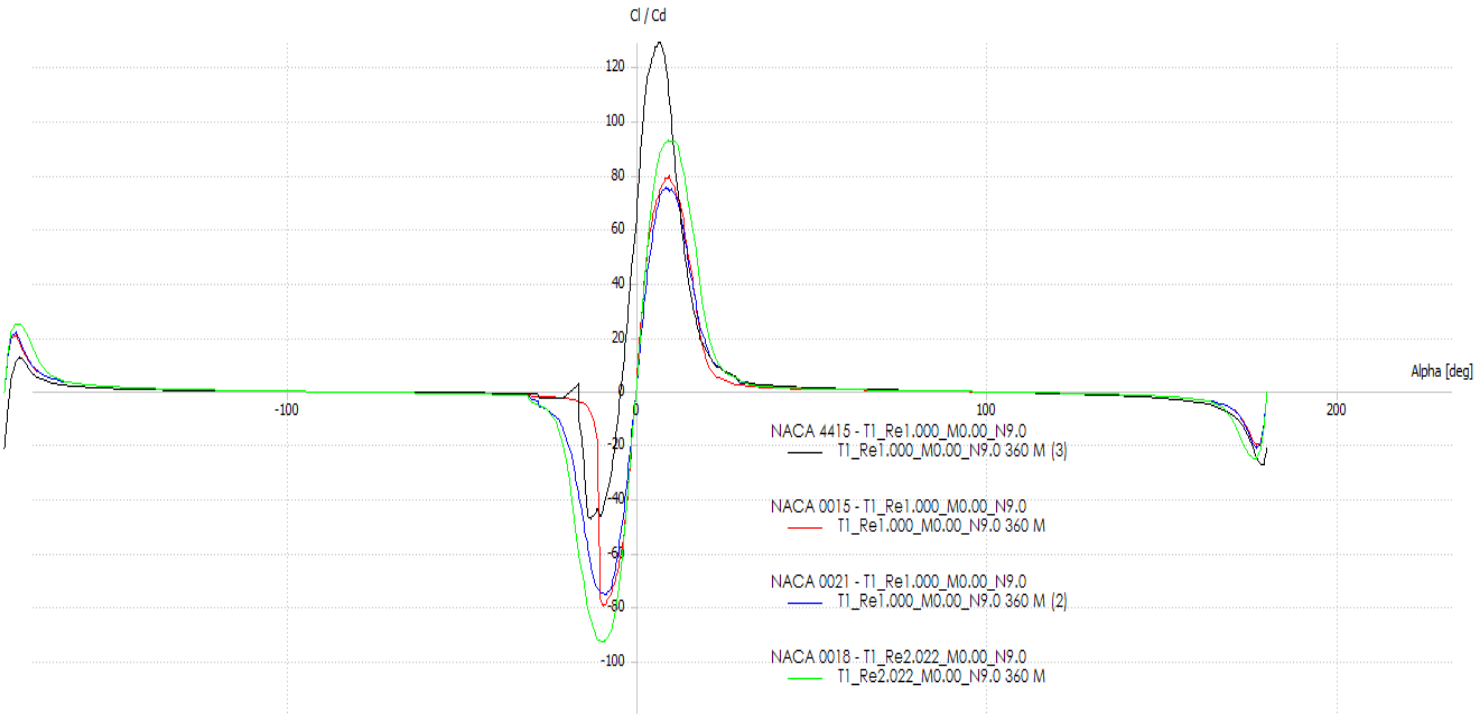

Figure 3.4 Cl/Cd graphs for NACA profiles under consideration.

3.1.3 Solidity:

Solidity (σ) is defined as the ratio between the total blade area and the projected turbine area (Tullis, Fiedler, McLaren, & Ziada). It is an important non dimensional parameter which affects self-starting capabilities and for VAWT (Vertical Axis Water Turbine) is calculated with:

$$\sigma = \frac{Nc}{R}$$

where N is the number of blades, c is the blade chord, it is considered that each blade sweeps the area twice. This formula is not applicable for HAWT as they have different shape of swept area.

Solidity determines when the assumptions of the momentum models are applicable, and only when using high $\sigma \geq 0.4$ a self-starting turbine is achieved.

Solidity	Chord
0.3	3.2385
0.32	3.4544
0.34	3.6703
0.36	3.8862
0.38	4.1021
0.4	4.318
0.42	4.5339
0.44	4.7498
0.46	4.9657
0.48	5.1816
0.5	5.3975
Table 3.1	

Before selecting the solidity, let us define another dimensionless factor called as Reynolds Number. Reynolds number define the type of fluid motion whether it's laminar or turbulent. Using Int J Energy Environ Eng (2014) 5:333–340 (figure 3.5) Research paper on vertical axis turbine, graphs of TSR vs Cp for particular Reynolds numbers and solidities were analyzed.

TSR = Tip speed ratio = $\lambda = \frac{r\omega}{v}$ is yet another dimensionless parameter which actually explains the relative speed of the blade compared with the speed of the fluid flowing. An optimum value of TSR is selected against the highest value of **Cp= Power Coefficient** so as to ensure maximum energy from water is extracted in the form of electric power. Since TSR is a function of solidity, a graph of it against Cp are well defined in the aforementioned research paper.

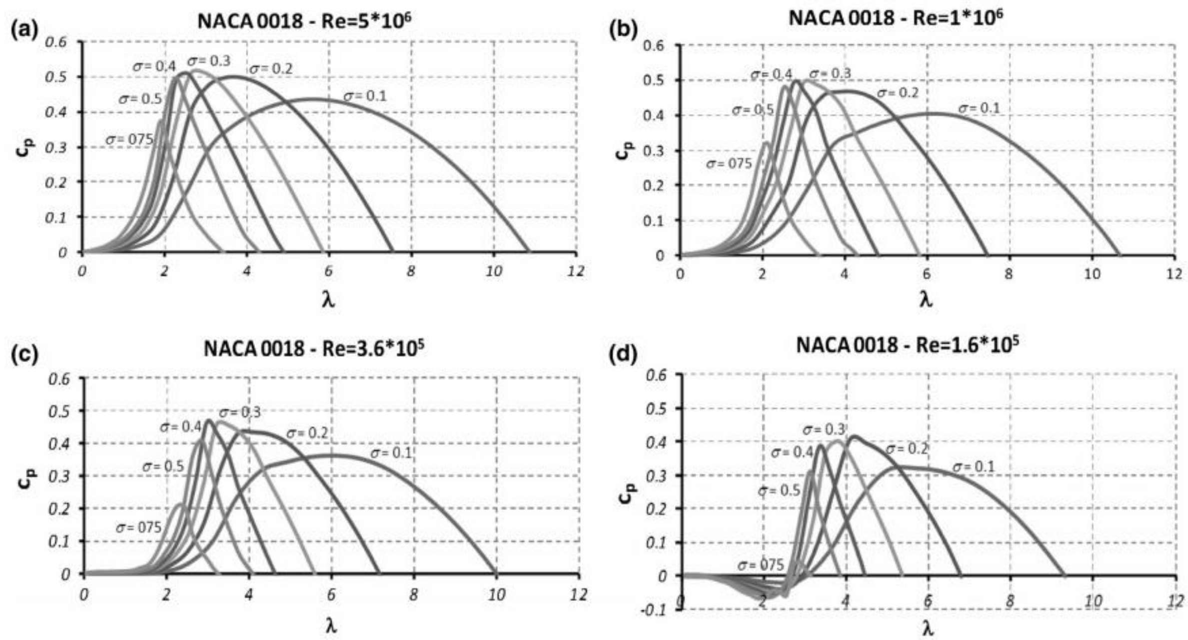

Figure 3.5 Cp vs λ graphs for particular solidities and Re.

Reynolds Number – another dimensionless number is defined as Re = $\frac{\rho V D p}{\mu}$

ρ = density of water,

V = velocity of water

D_p = Diameter of the pipe

μ = Dynamic viscosity of water.

For our design parameters and fluid properties at room temperature,

Re= 998*3*(36*0.0254)/(1.002E-3)

Re = 2.68 E 06

Going back to figure b, it is found that for σ = 0.4, with ƛ ≈ 3, maximum Cp is obtained. Since σ > 0.4 avoids starting torque problems, a higher value of σ = 0.5 is chosen. This was further attested from QBlade that optimum Cp was achieved for 2.75< ƛ < 3.75 (figure 3.6).

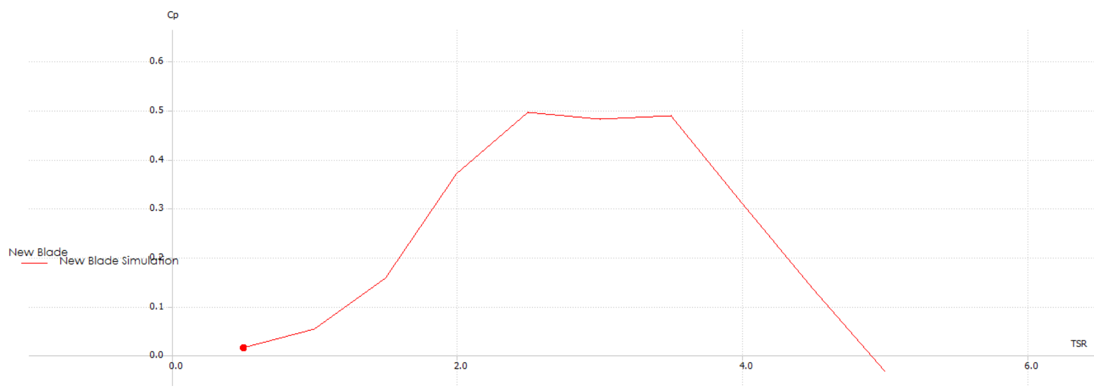

Figure 3.6 Cp vs ƛ graph for NACA 4415

Now that solidity is selected, chord length is thus calculated and is found to be 5.5 cm.

3.1.4 Number of Blades:

Another important factor in determining the chord length was the number of blades. The numbers of blades used to calculate the chord length were selected to be 4 for reasons mentioned below.

Again QBlade was used to find the best number of blades that could be used for the turbine.

Below is a graph of a Cp vs ƛ for varying number of blades of turbine. It is can be seen that the graph for 4 blades always tops that of the 3 blades. However, the graph for 5 blades peaks above both of them for a certain range and yet the peak value for all three blades is of 4 blade turbine. Since the range is too small which means that for very small range of velocities it is applicable.

Adding the cost of manufacturing another blade as well as the fact that it will cause even more pressure drop, the number of blades were chosen to be 4.

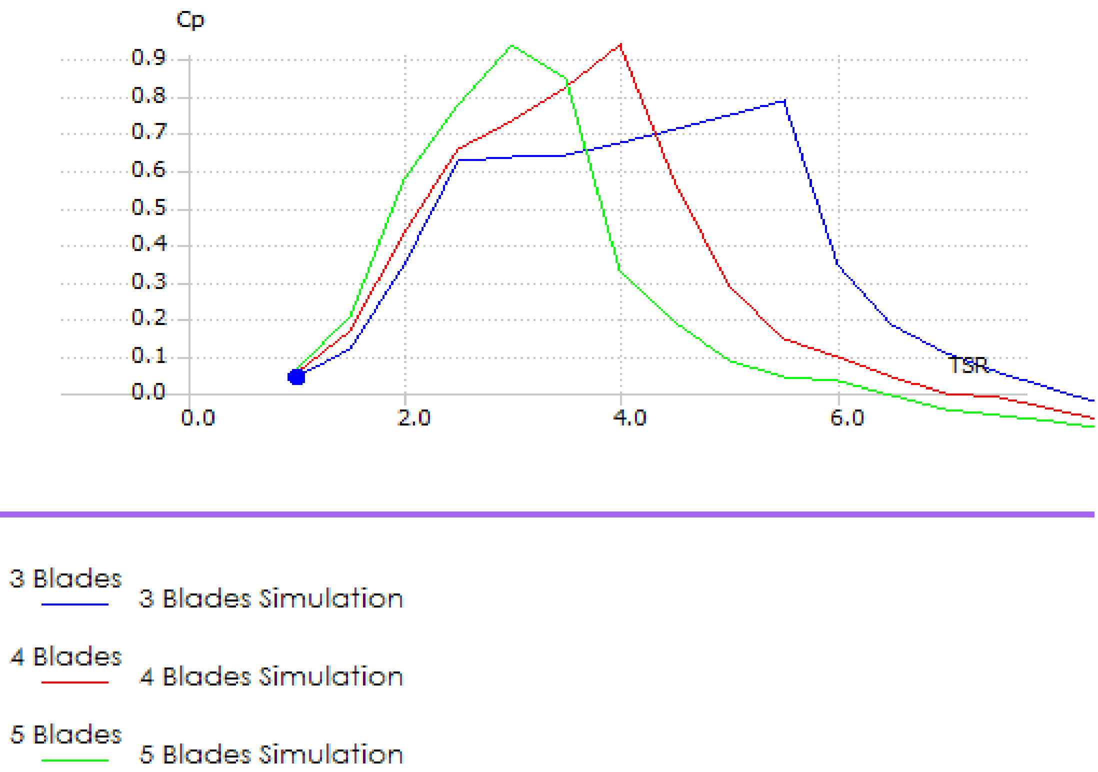

Figure 3.7 Cp vs λ graph for varying no. of blades

Having designed the turbine, the next step was to test further simulations for power generation, torque requirement, fluid analysis etc.

QBlade was again used for further simulations.

Design parameters are finalized as mentioned below:

Symbol	Parameter	Value
Air foil	NACA Profile	NACA 4415
D_p	Diameter of Pipe	36 inches
D_t	Diameter of Turbine	34 inches
V	Fluid Velocity	3 m/s
H	Blade Height	34 inches
R	Blade Radius	17 inches
λ	TSR	3.0
σ	Solidity	0.5
N	Number of Blade	4
C	Chord Length	5.5 cm

Table 3.2

Complete simulation of all aspects of the turbine and the resulting graphs are plotted below:

3.2 Turbine Design (Original):

3.2.1 NACA 4415:

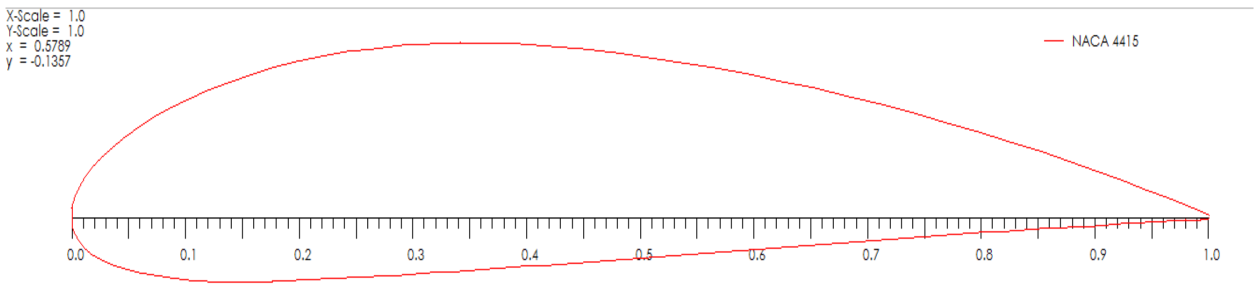

Figure 3.8 NACA 4415

3.2.2 Cl/Cd Ratio Graph:

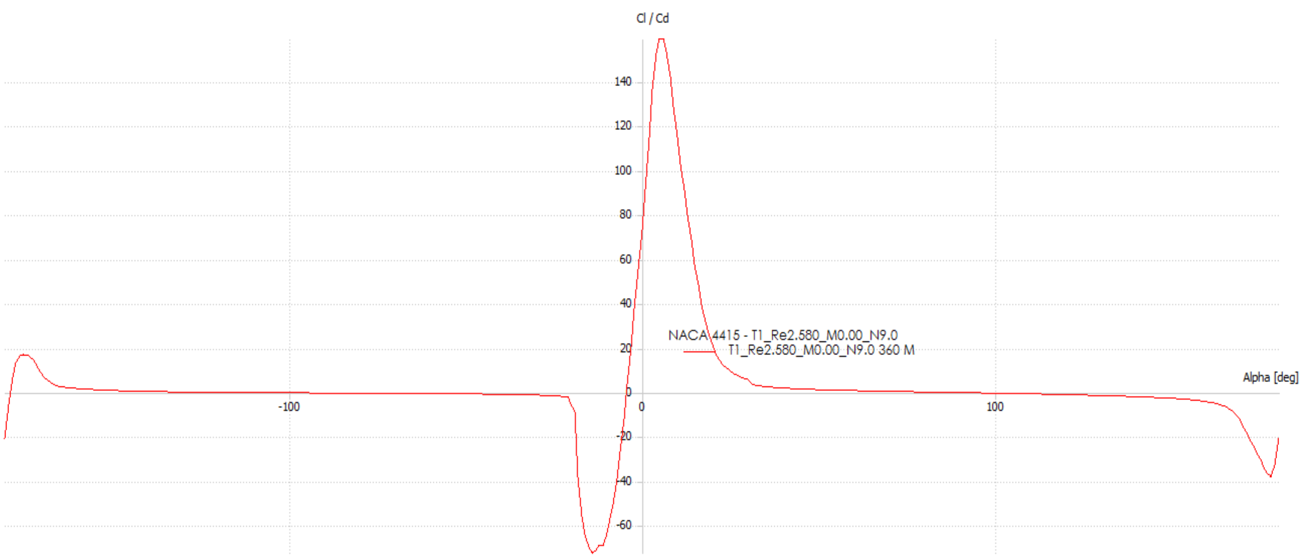

Figure 3.9 Cl/Cd vs α graph for NACA 4415

3.2.3 A view of the Turbine profile input parameters:

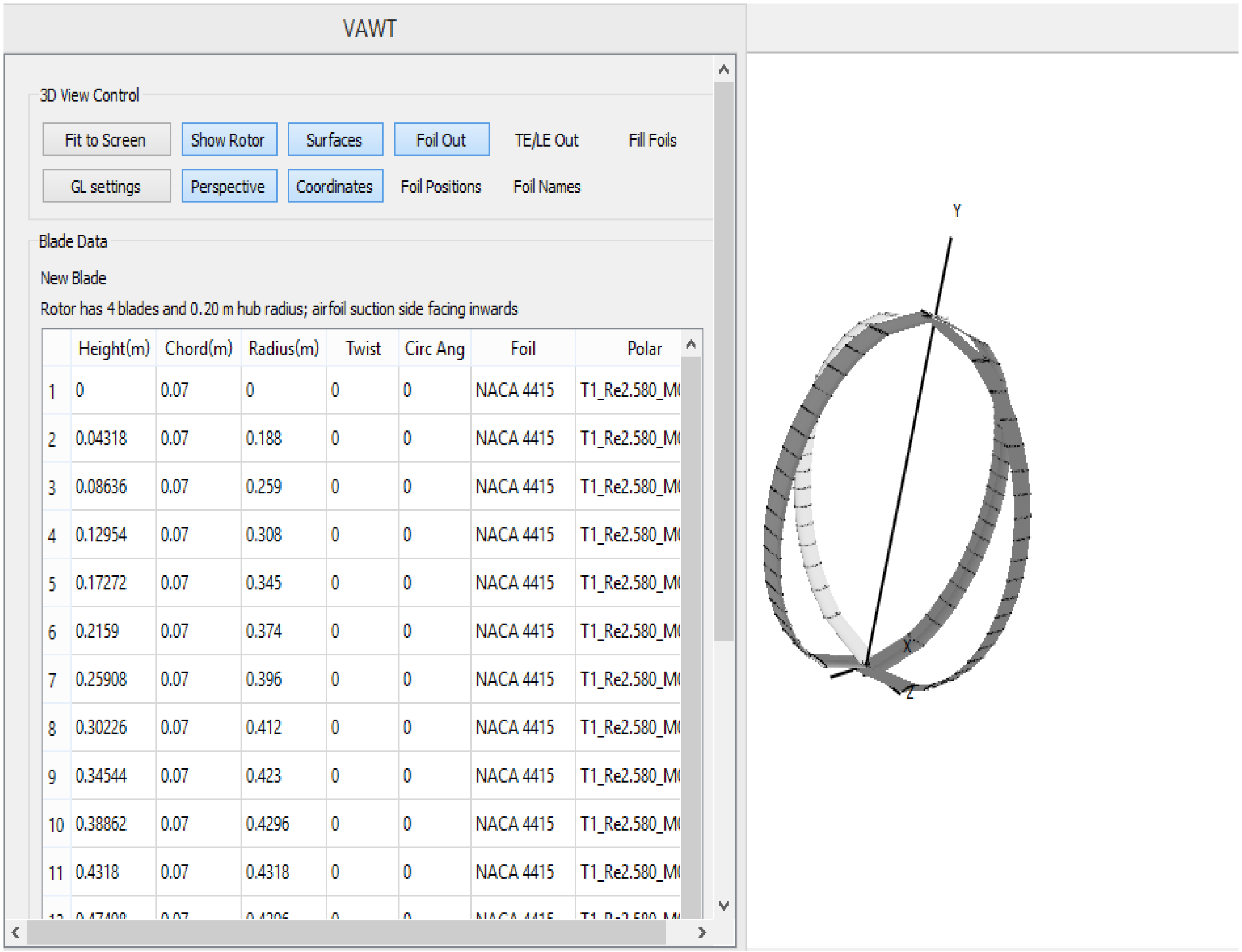

	Height(m)	Chord(m)	Radius(m)	Twist	Circ Ang	Foil	Polar
1	0	0.07	0	0	0	NACA 4415	T1_Re2.580_M
2	0.04318	0.07	0.188	0	0	NACA 4415	T1_Re2.580_M
3	0.08636	0.07	0.259	0	0	NACA 4415	T1_Re2.580_M
4	0.12954	0.07	0.308	0	0	NACA 4415	T1_Re2.580_M
5	0.17272	0.07	0.345	0	0	NACA 4415	T1_Re2.580_M
6	0.2159	0.07	0.374	0	0	NACA 4415	T1_Re2.580_M
7	0.25908	0.07	0.396	0	0	NACA 4415	T1_Re2.580_M
8	0.30226	0.07	0.412	0	0	NACA 4415	T1_Re2.580_M
9	0.34544	0.07	0.423	0	0	NACA 4415	T1_Re2.580_M
10	0.38862	0.07	0.4296	0	0	NACA 4415	T1_Re2.580_M
11	0.4318	0.07	0.4318	0	0	NACA 4415	T1_Re2.580_M

Figure 3.10 A view of the Turbine profile input parameters:

3.2.4 Power vs TSR:

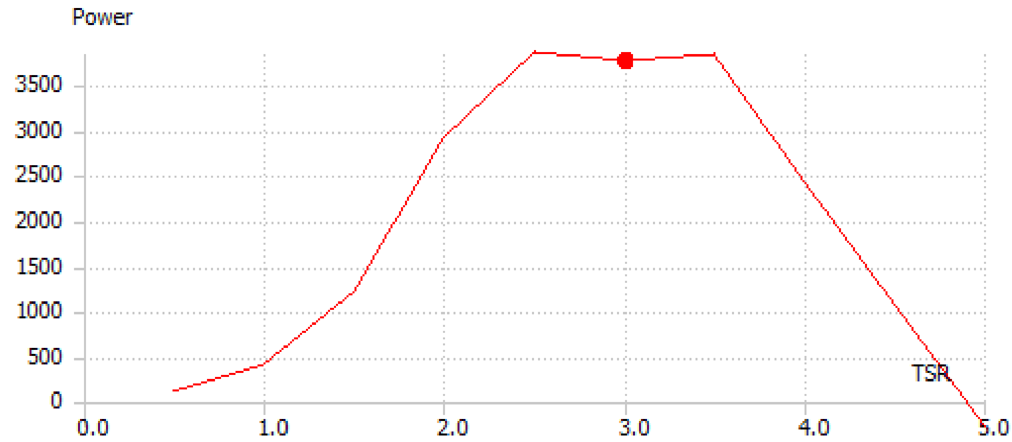

Figure 3.11 Power vs TSR graph for NACA 4415

Qblade predicts that the designed turbine will be able to produce upto 3.5KW of power for our current design parameters. The result will later be substantiated by analytical method as well using Matlab.

3.2.5 Torque vs TSR:

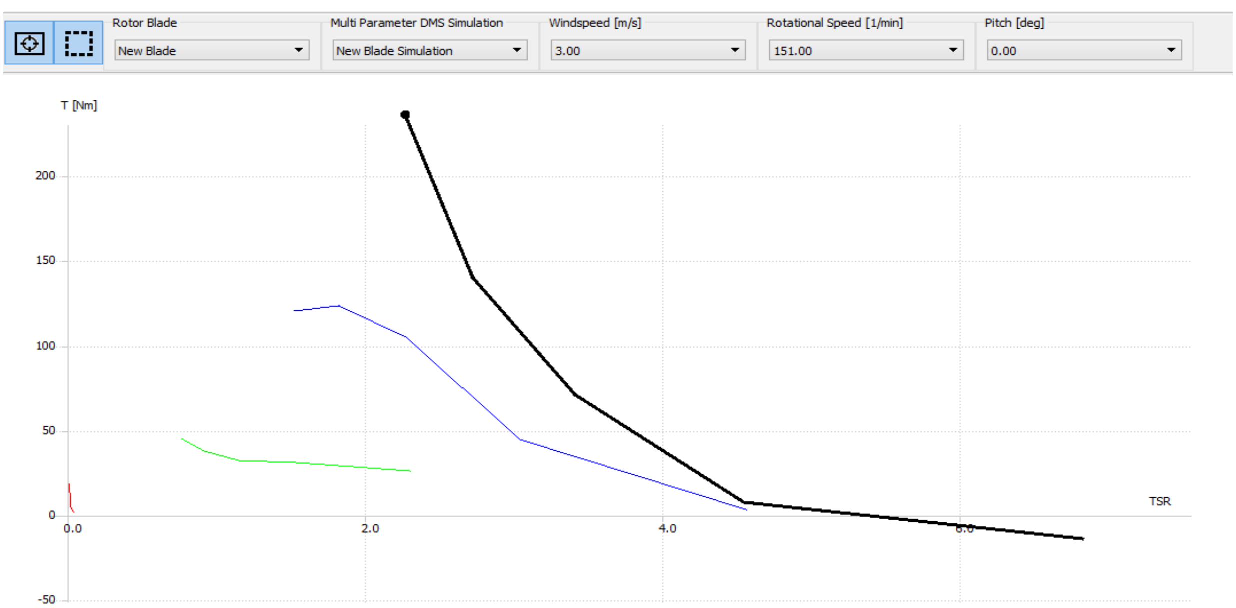

Figure 3.12. Torque vs TSR graph for NACA 4415

Having conducted the simulation for the original turbine, it was now required to calculate numerous other parameters as well of the turbine using analytical technique so as to verify the results of the software used above.

3.3 Mathematical Model:

A Matlab program was developed using BEM theory to calculate various forces generated across the foil and the resulting torque and the revolutions of the rotor.

3.3.1 BEM Theory: (Literature Review)

Blade element momentum theory is a theory that combines both blade element theory and momentum theory. It is used to calculate the local forces on a propeller or wind-turbine blade. Blade element theory is combined with momentum theory to alleviate some of the difficulties in calculating the induced velocities at the rotor.

Blade element momentum theory accounts for the angular momentum of the rotor. Consider the left hand side of the figure below. We have a stream tube, in which there is the fluid and the rotor. We will assume that there is no interaction between the contents of the stream tube and everything outside of it. That is, we are dealing with an isolated system. In physics, isolated systems must obey conservation laws. An example of such is the conservation of angular momentum. Thus, the angular momentum within the stream tube must be conserved. Consequently, if the rotor acquires angular momentum through its interaction with the fluid, something else must acquire equal and opposite angular momentum. As already mentioned, the system consists of just the fluid and the rotor, the fluid must acquire angular momentum in the wake. As we related the change in axial momentum with some induction factor a’, we will relate the change in angular momentum of the fluid with the tangential induction factor, $a_{z'}$.

Let us consider the following setup.

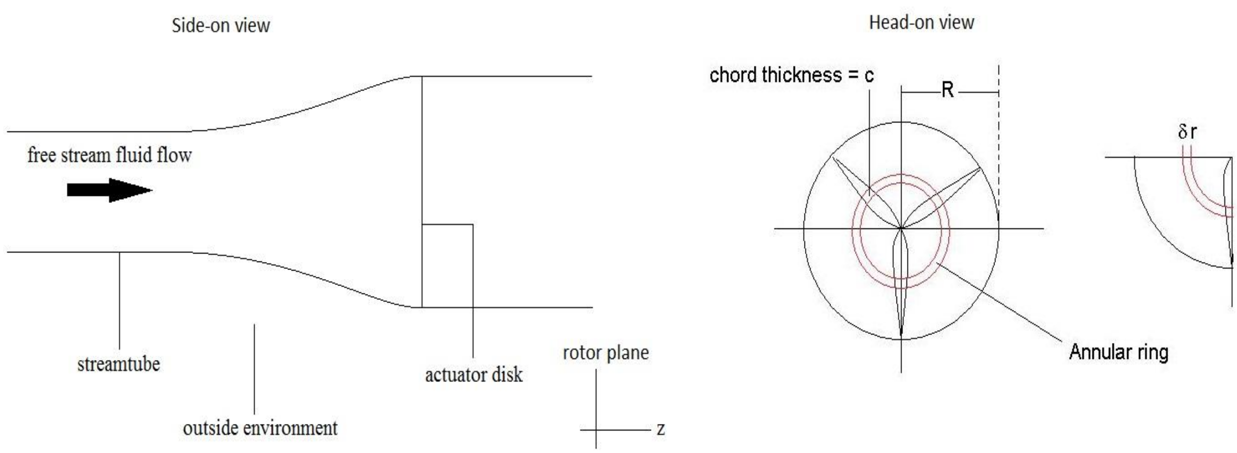

Figure 3.13 Rotor area

We will break the rotor area up into annular rings of infinitesimally small thickness. We are doing this so that we can assume that axial induction factors and tangential induction factors are constant throughout the annular ring. An assumption of this approach is that annular rings are independent of one another i.e. there is no interaction between the fluids of neighboring annular rings.

Bernoulli for rotating wake

Let us now go back to Bernoulli:

$$\frac{1}{2}\rho v_1^2 + P_1 = \frac{1}{2}\rho v_2^2 + P_2$$

The velocity is the velocity of the fluid along a streamline. The streamline may not necessarily run parallel to a particular co-ordinate axis, such as the z-axis. Thus the velocity may consist of components in the axes that make up the co-ordinate system. For this analysis, we will use cylindrical polar co-ordinates (r, Ɵ, z). Thus

$$v^2 = v_r^2 + v_\theta^2 + v_z^2 .$$

NOTE: We will in fact, be working in cylindrical co-ordinates for all aspects e.g.

$$\mathbf{F} = F_r\hat{\mathbf{r}} + F_\theta\hat{\theta} + F_z\hat{\mathbf{z}}$$

Now consider the setup shown above. As before, we can break the setup into two components: upstream and downstream.

Pre-rotor:

$$P_\infty + \frac{1}{2}\rho v_u^2 = P_{D+} + \frac{1}{2}\rho v_D^2$$

where $\upsilon_{\grave{u}}$ is the velocity of the fluid along a streamline far upstream, and υ_D is the velocity of the fluid just prior to the rotor. Written in cylindrical polar co-ordinates, we have the following expression:

$$P_\infty + \frac{1}{2}\rho v_\infty^2 = P_{D+} + \frac{1}{2}\rho(v_\infty(1-a))^2$$

Where υ_∞ and υ_∞(1-a) are the z-components of the velocity far upstream and just prior to the rotor respectively. This is exactly the same as the upstream equation from the Betz model.

It should be noted that, as can be seen from the figure above, the flow expands as it approaches the rotor, a consequence of the increase in static pressure and the conservation of mass. This would imply that $\upsilon_r \neq 0$ upstream. However, for the purpose of this analysis, that effect will be neglected.

Post-rotor:

$$P_{D-} + \frac{1}{2}\rho v_D^2 = P_\infty + \frac{1}{2}\rho v_w^2$$

where υ_D is the velocity of the fluid just after interacting with the rotor. This can be written as

$$v_D^2 = v_{D,\ r}^2 + v_{D,\ \theta}^2 + v_{D,\ z}^2 .$$

The radial component of the velocity will be zero; this must be true if we are to use the annular ring approach; to assume otherwise would suggest interference between annular rings at some point downstream. Since we assume that there is no change in axial velocity across the disc, $\upsilon_{D\,,\,z}$ = (1-a)υ_∞. Angular momentum must be conserved in an isolated system. Thus the rotation of the wake must not die away. Thus υ_Θ in the downstream section is constant. Thus Bernoulli simplifies in the downstream section:

$$P_{D-} + \frac{1}{2}\rho v_{D,\ z}^2 = P_\infty + \frac{1}{2}\rho v_{w,\ z}^2 = P_{D-} + \frac{1}{2}\rho(v_\infty(1-a))^2$$

In other words, the Bernoulli equations up and downstream of the rotor are the same as the Bernoulli expressions in the Betz model. Therefore, we can use results such as power extraction and wake speed that were derived in the Betz model i.e.

$$v_{w,z} = (1-2a)v_\infty$$

$$\text{Power} = 2a(1-a)^2 v_\infty^3 \rho A_D$$

This allows us to calculate maximum power extraction for a system that includes a rotating wake. This can be shown to give the same value as that of the Betz model i.e. 0.59. This method involves recognizing that the torque generated in the rotor is given by the following expression:

$$\delta\mathbf{Q} = 2\pi r\delta r \times \rho U_\infty(1-a) \times 2a' r\omega$$

Blade forces:

Consider fluid flow around an airfoil. The flow of the fluid around the airfoil gives rise to lift and drag forces. By definition, lift is the force that acts on the airfoil normal to the apparent fluid flow speed seen by the airfoil. Drag is the forces that acts tangential to the apparent fluid flow speed seen by the airfoil. What do we mean by an apparent speed? Consider the diagram below:

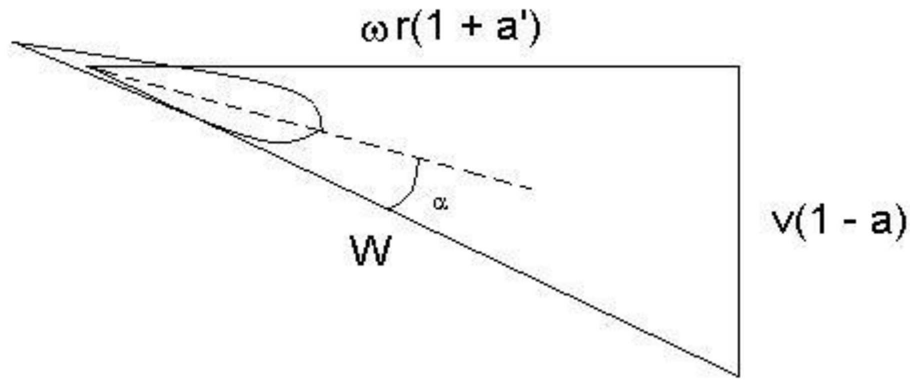

Figure 3.14 Velocity Triangle

The speed seen by the rotor blade is dependent on three things: the axial velocity of the fluid, υ_∞(a-1); the tangential velocity of the fluid due to the acceleration round an airfoil a'ώr; and the rotor motion itself, ώr. That is, the apparent fluid velocity is given as below:

$$\mathbf{v} = \omega r(1 + a')\hat{\theta} + v_\infty(1 - a)\hat{\mathbf{z}}$$

Thus the apparent wind speed is just the magnitude of this vector i.e.:

$$|\mathbf{v}|^2 = (\omega r(1 + a'))^2 + (v_\infty(1 - a))^2 = W^2$$

We can also work out the angle Ø from the above figure:

$$\sin\phi = \frac{v_\infty(1 - a)}{W}$$

Supposing we know the angle β, we can then work out α simply by using the relation α = Ø - β; we can then work out the lift co-efficient, C_l, and the drag co-efficient C_d, from which we can work out the lift and drag forces acting on the blade.

Consider the annular ring, which is partially occupied by blade elements. The length of each blade section occupying the annular ring is δr (see figure below).

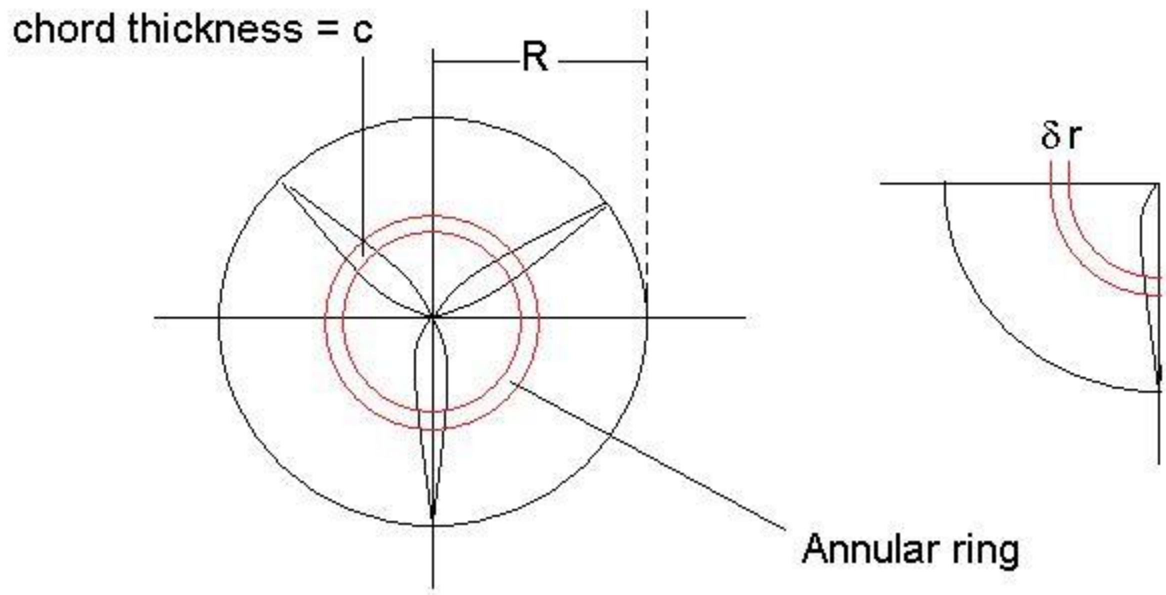

Figure 3.15 Blade Cross Section

The lift acting on those parts of the blades/airfoils each with chord c is given by the following expression:

$$\delta L = \frac{1}{2}\rho N W^2 c \times c_L(\alpha)\delta r$$

where C_l is the lift co-efficient, which is a function of the angle of attack, and N is the number of blades. Additionally, the drag acting on that part of the blades/airfoils with chord c is given by the following expression:

$$\delta D = \frac{1}{2}\rho N W^2 c \times c_D(\alpha)\delta r$$

Remember that these forces calculated are normal and tangential to the apparent speed. We are interested in forces in the z and Θ axes. Thus we need to consider the diagram below:

Thus we can see the following:

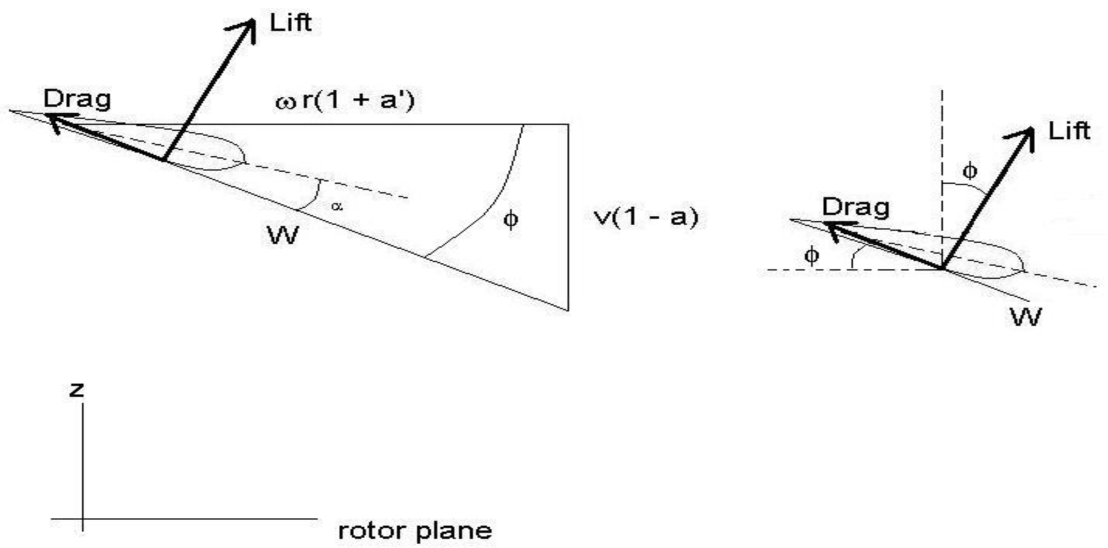

Figure 3.16 Velocity Triangle

$$\delta F_\theta = \delta L \sin\phi - \delta D \cos\phi$$

$$\delta F_z = \delta L \cos\phi + \delta D \sin\phi$$

F_Θ is the force that is responsible for the rotation of the rotor blades; F_z is the force that is responsible for the bending of the blades.

Recall that for an isolated system the net angular momentum of the system is conserved. If the rotor acquired angular momentum, so must the fluid in the wake. Let us suppose that the fluid in the wake acquires a tangential velocity $\upsilon_\Theta = 2a'\dot{\omega}r$. Thus the torque in the air is given by

$$|\delta \mathbf{Q}| = \rho(2\pi r \delta r)U_\infty(1-a) \times (2\Omega a' r^2)$$

By the conservation of angular momentum, this balances the torque in the blades of the rotor; thus,

$$\frac{1}{2}\rho W^2 Nc(c_l \sin\phi - c_d \cos\phi) r\delta r = \rho(2\pi r\delta r)U_\infty(1-a) \times (2\Omega a' r^2)$$

$$\frac{1}{2}W^2 Nc(c_l \sin\phi - c_d \cos\phi) = 4\pi U_\infty(1-a) \times \Omega a' r^2$$

Furthermore, the rate of change of linear momentum in the air is balanced by the out-of-plane bending force acting on the blades, δF_z. From momentum theory, the rate of change of linear momentum in the air is as follows:

$$\delta F_z = \rho(2\pi r\delta r)U_\infty(1-a) \times (v_\infty - v_w)$$

which may be expressed as

$$\delta F_z = \rho(4\pi r\delta r)U_\infty^2 a(1-a)$$

Balancing this with the out-of-plane bending force gives

$$\frac{1}{2}W^2 Nc(c_l \cos\phi + c_d \sin\phi) = \rho(4\pi r\delta r)U_\infty^2 a(1-a)$$

Let us now make the following definitions:

$$C_y = c_l \sin\phi - c_d \cos\phi$$

$$C_x = c_l \cos\phi + c_d \sin\phi$$

So we have the following equations:

$$\frac{1}{2}W^2NcC_y = 4\pi U_\infty(1-a)\times\Omega a' r^2$$

$$\frac{1}{2}\rho W^2NcC_x = 4\pi\rho\left[(a'\Omega r)^2 + U_\infty^2 a(1-a)\right] r$$

Let us make reference to the following equation which can be seen from analysis of the above figure:

$$\sin\phi = \frac{U_\infty}{W}(1-a) \rightarrow \sin^2\phi = \left(\frac{U_\infty}{W}(1-a)\right)^2$$

Thus, with these three equations, it is possible to get the following result through some algebraic manipulation:

$$\frac{a}{1-a} = \frac{C_x\sigma_r}{4\sin^2\phi}$$

We can derive an expression for a’ in a similar manner. This allows us to understand what is going on with the rotor and the fluid. Equations of this sort are then solved by iterative techniques.

3.3.2 Matlab Program:

The Matlab program written below yields the results of the program for the turbine are mentioned below in table 3.3, and the graphical representations of them in figure 3.17:

```
clear all
clc

fprintf('Hydrodynamics of Vertical Axis Water Turbine (2D Analysis)\n');


clc

%Properties
```

```
rho      =   1000;    %Density of water [kg/m^3]
kv       =   1e-6;    %Kinematic viscoity of Water [m^2/s]
V        =   0.6;       %Free stream velocity of Water [m/s]
%R        =   36*.0254/2;    %Turbine Rotor radius [m]
%V        =   (36/28)^2*V1;    %Reduced dia velocity - Venturi Effect
%h        =   36*.0254;    %Turbine Height [m]
dtheta   =   1;       %Difference between interval [degree]
i        =   1;       %Interval integer
k=1:180;
angle    =   dtheta*k*pi/180;%radians
angle_d =   dtheta*k;
grad     =   0.11;   %*pi/180;


%Input

 prompt   =   '\n\nEnter the value of Height of turbine blades in inches\n\n
';
 h      =   input(prompt);
 h       =   h*.0254;

 prompt   =   'Enter the value of diameter of pipe in inches\n\n  ';
 d      =   input(prompt);
 R       =   d*0.0254/2;


 prompt   =   'Enter the value of Tip speed Ratio\n\n  ';
 TSR      =   input(prompt);

 prompt   =   'Enter the number of blades \n \n ';
 N        =   input(prompt);

 prompt   =   'Enter the value of chord length \n \n ';
 c        =   input(prompt);

Area        =  2*R*h;

[A,B,C]     =   xlsread('myfile.xlsx');      %Lift and drag coefficient
reading from excel

Cl1      =   A(:,2);
Cl       =   Cl1';

Cd1      =   A(:,3);
Cd       =   Cd1';
%Relations
sigma        =    (N*c)/(R);          %Solidity


    au       =    (sigma*grad*TSR)/(16)  %Induction Factor
    Va       =    V*(1-au);
    w        =    (TSR*Va)/R;
    for i=1:1:180
```

```
        Vc(i)          =   w*R+Va*cos(angle(i));  %Tangential Velocity
        Vn(i)          =   Va*sin(angle(i));
        W(i)           =   (Vc(i)^2+Vn(i)^2)^0.5;       %Relative Velocity

        %W(i)         =   V*(1+2*TSR*cos(angle(i))+TSR^2)^0.5; % Relative
Velocity

        mub(i)       =  sin(angle(i))/(TSR+cos(angle(i)));

        Aoa(i)       =   atan(mub(i));

        Re(i)        =   c*W(i)/kv;

        %Cn(i)        =   (Cl(i)*cos(Aoa(i)))+(Cd(i)*sin(Aoa(i)));

        %Ct(i)        =   (Cl(i)*sin(Aoa(i)))-(Cd(i)*cos(Aoa(i)));

        Fl(i)        =   0.5*rho*Cl(i)*(W(i)^2)*c*h;

        Fd(i)        =   0.5*rho*Cd(i)*(W(i)^2)*c*h;

        Fn(i)       =   Fl(i)*cos(Aoa(i))+Fd(i)*sin(Aoa(i));

        Ft(i)        =   Fl(i)*sin(Aoa(i))-Fd(i)*cos(Aoa(i));

        Torque(i)    =   Ft(i)*R*N;

        i=i+1;

    end
    V2 = V*(1-2*au);   %downstream velocity
    P_loss = (0.5*rho*(V^2-V2^2))/10000;

    %Summation and Calculations of Final Results
Ft_avg  =   mean(Ft);
Fn_avg  =   mean(Fn);
Fl_avg  =   mean(Fl);
Fd_avg  =   mean(Fd);
Ft_max  =   max(Ft);
Fl_max  =   max(Fl);
Q_max   =   max(Torque);
Q       =   Ft_avg*N*R;     % Average Torque
w       =   TSR*V/R;        % Angular Velocity
w1       =   TSR*V*60/(R*2*3.1428);
P       =   Q*w;            % Power Output
Pi      =   0.5*rho*Area*V^3;
cop      =   P/Pi;


%Graphs

subplot(3,2,1)
```

```
plot(angle_d,Aoa*180/pi)
ylabel('Angle of attack');
%legend('TSR = 1');

subplot(3,2,2)
plot(angle_d,Fl)
ylabel('Lift Force');

subplot(3,2,3)
plot(angle_d,Fd)
ylabel('Drag Force ');

subplot(3,2,4)
plot(angle_d,Torque)
ylabel('Torque');

subplot(3,2,5)
plot(angle_d,Ft)
ylabel('Thrust Force');

subplot(3,2,6)
plot(angle_d,Fn)
ylabel('Normal Force');

%Results to be displayed

fprintf('\n\nVAWT Results\n\n');
fprintf('\n\nThe input/available power is %f\n\n',Pi);
fprintf('The average Torque is %f [N.m]:\n\n',Q);
fprintf('The average Lift Force is %f [N] \n\n',Fl_avg);
fprintf('The average Drag Force is %f [N] \n\n',Fd_avg);
fprintf('The average Thrust Force is %f [N] \n\n',Ft_avg);
fprintf('The average Normal Force is %f [N] \n \n',Fn_avg);
fprintf('The maximum value of Torque is %f \n\n',Q_max);
fprintf('The maximum value of Lift Force is %f \n\n',Fl_max);
fprintf('The maximum value of Thrust force is %f \n\n',Ft_max);
fprintf('The angular velocity of blades is %f [RPM]\n\n',w1);
fprintf('The solidity of turbine  is %f \n\n',sigma);
fprintf('Heaad loss across turbine is  %f [m]\n\n',P_loss);
fprintf('The power output of VAWT is %f \n\n',P);
fprintf('The Coefficient of Power of VAWT is %f\n\n',cop);
```

```
%This function calculates the power coefficient and average torque
%for a vertical axis wind turbine according to the procedure stated at:
%"Double-Multiple Streamtube model for Darrieus wind turbines,
%I.Paraschivoiu", the equations have been adapted to a straight bladed
%wind turbine when necessary.
function [Cpt, av_T] = f_Cp_and_av_T2 (Vo, w, R, N, c, L, Ao, NACA)
%%INPUT PARAMETERS
%Vo = ambient air speed (m/s).
%w = rotor angular speed (rad/s).
%R = rotor radius (m).
%N = number of blades.
```

```
%c = blade chord (m).
%L = blade length (m).
%Ao = initial angle of attack (rad).
%NACA = airfoil used (15 or 21).
%%OUTPUT PARAMETERS
%Cpt = power coefficient.
%av_T = average torque (Nm).
%%CONSTANTS FOR STANDARD AIR CONDITIONS AND SEA LEVEL
kv = 1e-6; % Kinematic viscosity at 15°C [m^2/s].
rho = 1000; % air density (Standard density at sea level)[kg/m^3]
%%OTHER PARAMETERS
n=36; % number of streamtubes (180/5) divides one half of the rotor in 5°
% increments.
% theta = vector containing the angles between streamtube and local radius
% to the rotor axis.
thetau = linspace (-89*pi/180, 89*pi/180, n); % upstream angles (rad).
thetad = linspace (91*pi/180, 269*pi/180, n); % downstream angles (rad).
Xt = w*R/Vo; %Tip speed ratio

S = 2*L*R; %Swept area [m^2]
%%--------------- UPSTREAM CALCULATION ---------------------
%%Get the corresponding au value for each streamtube (each theta value)
i = 0; %initialize the counter value
while (i~=n)
i = i+1;
au = 1.01; % velocity induction factor upstream.
newau = 1; % initialize, au must be different from newau
while ((au-newau)>1e-3) %Iterative process to find au
au = newau;
Vu = Vo*(au); %Vu =velocity upstream of wind turbine cylinder
X = R*w/Vu; %Local Tip speed ratio
% Wu=local resultant air velocity
Wu = sqrt ( Vu^2*( (X - sin (thetau(i)))^2 + (cos (thetau(i)))^2));
Reb = Wu*c/kv; %Blade Reynolds number
% the values from airfoil lift and drag coefficients depending on
% the angle of attack are interpolated for the given Reynolds num-
% ber
if (NACA==15)
[A1, Cl1, Cd1] = NACAfinder15 (Reb); %NACA0015
else
[A1, Cl1, Cd1] = NACAfinder21 (Reb); %NACA0021
end
costh = cos(thetau(i));
cosao = cos(Ao);
sinth = sin(thetau(i));
sinao = sin(Ao);
A = asin((costh*cosao-(X-sinth)*sinao)/sqrt((X-sinth)^2+(costh^2)));
% if angle of attack is negative the sign is changed for interpolating
%in the data tables and then the lift coefficient sign is
% changed.
neg = 0;
if (sign(A)==-1)
neg = 1;
end
A = abs(A*180/pi); %Conversion to degrees to match table
Cl = interp1 (A1, Cl1, A, 'linear');
Cd = interp1 (A1, Cd1, A, 'linear');
```

```
if (neg==1)
A = -1*A; %Restablish the original value for plots
Cl =-1*Cl;
Cd =1*Cd;
end
% Cn = normal coefficient, % Ct = tangential coefficient
Cnu = Cl*cosd (A) + Cd*sind (A); %note that A is in degrees
Ctu = Cl*sind (A) - Cd*cosd (A);
% fup = function to find interference factor (au).
g=@(thetau) (abs(sec (thetau)).*(Cnu.*cos(thetau)-
Ctu.*sin(thetau)).*(Wu./Vu).^2);
y = quadl (g, -89*pi/180, 89*pi/180);
fup = N*c*y/(8*pi*R);
%[newau] = solve ('fup*newau = pi*(1-newau)')
%syms newau
%S1 = solve ('fup*newau*R = pi*(1-newau)*r(k)', 'newau')
newau = pi/(fup+pi); % new interference factor value for the next
% iteration process.
end

Auvector (i) = A; % Store angle of attack value
auvector (i) = newau; % Store au value in a vector
Fnu (i) = (c*L/S)*Cnu*(Wu/Vo)^2; % normal force coefficient
Ftu (i) = (c*L/S)*Ctu*(Wu/Vo)^2; % tangential force coefficient
Tup (i) = 0.5*rho*c*R*L*Ctu*Wu^2; % torque produced in when the blade
% crosses this streamtube
end
% Average upstream torque
ts2 = f_trapezoidal_integration_s (thetau, Tup)
av_Tup = N*(ts2)/(2*pi) %upstream average torque
% Average torque coefficient
av_Cqu = av_Tup/(0.5*rho*S*R*Vo^2)
Cpu = av_Cqu*Xt; %upstream power coefficient
%%--------------- DOWNSTREAM CALCULATION ---------------------
j = n+1;
flag =0;
i = 0; %initialize the counter value
while (j~=1)
j = j-1;
i = i+1; % interference factor downstream.
ad = 1.01; % velocity induction factor upstream.
newad = auvector(j); % initialize, au must be different from newau
while ((ad-newad)>1e-3) %Iterative process to find ad
ad = newad;
Ve = Vo*((2*auvector(j))-1); %Ve = air velocity inside cylinder
Vd = Ve*ad; %Vd = air velocity downstream of cylinder
X = R*w/Vd; %Local Tip speed ratio
% Wd=local resultant air velocity

Wd = sqrt ( Vd^2*( (X - sin (thetad(i)))^2 + (cos (thetad(i)))^2));
Reb = Wd*c/kv; %Reynolds number of the blade
if (NACA==15)
[A1, Cl1, Cd1] = NACAfinder15 (Reb);
else
[A1, Cl1, Cd1] = NACAfinder21 (Reb);
end
```

```
costh = cos(thetad(i));
cosao = cos(Ao);
sinth = sin(thetad(i));
sinao = sin(Ao);
A = asin((costh*cosao-(X-sinth)*sinao)/sqrt((X-sinth)^2+(costh^2)));
neg = 0;
if (sign(A)==-1)
neg = 1;
end
A = abs(A*180/pi); %Conversion to degrees to match table
Cl = interp1 (A1, Cl1, A, 'linear');
Cd = interp1 (A1, Cd1, A, 'linear');
if (neg==1)
A = -1*A; %Restablish the original value for plots
Cl =-1*Cl;
Cd =1*Cd;
end
% Cn = normal coefficient, % Ct = tangential coefficient
Cnd = Cl*cosd (A) + Cd*sind (A); %note that A is in degrees
Ctd = Cl*sind (A) - Cd*cosd (A);
g=@(thetad) (abs(sec (thetad)).*(Cnd.*cos(thetad)-
Ctd.*sin(thetad)).*(Wd./Vd).^2);
y = quadl (g, 91*pi/180, 269*pi/180);
fdw = N*c*y/(8*pi*R);
%[newau] = solve ('fup*newau = pi*(1-newau)')
%syms newau
%S1 = solve ('fup*newau*R = pi*(1-newau)*r(k)', 'newau')
if (flag ==0)
newad = pi/(fdw+pi);
end
%if the iteration process does not converge, the value of the
%interference factor upstream from the same streamtube is taken
if (newad<0.01)
warning('newad<0.01 at theta = %d and A = %d', (thetad(i)*180/pi),A);
if (i>1)
newad = advector(i-1);
else
newad = auvector (i);
end
flag = 1;
end
end
Advector (i) = A;
advector (i) = newad; %Store ad value in a vector
% Force coefficients and torque calculation
Fnd (i) = (c*L/S)*Cnd*(Wd/Vo)^2;
Ftd (i) = (c*L/S)*Ctd*(Wd/Vo)^2;
Tdw (i) = 0.5*rho*c*R*L*Ctd*Wd^2;
end
% Average upstream torque
ts4 = f_trapezoidal_integration_s (thetad, Tdw)
av_Tdw = N*(ts4)/(2*pi) % upstream average torque
% Average torque coefficient
av_Cqd = av_Tdw/(0.5*rho*S*R*Vo^2)
Cpd = av_Cqd*Xt; % downstream power coefficient
Cpt = Cpd+Cpu % Total power coefficient
av_T = av_Tup + av_Tdw % Total average torque [Nm]
```

```
clc
clear all
[A,B,C]    =   xlsread('0018data.xlsx');
x=A(1,1);
y=A(63,1);
z=A(125,1);
k=1:180;
R        =   10*.0254/2;
angle    =   k*pi/180;
kv=1e-6;
rho=1000;
Va=2;
w        =   (2*Va)/R;
for i=1:180
    Vc(i)          =   w*R+Va*cos(angle(i));  %Tangential Velocity
    Vn(i)          =   Va*sin(angle(i));
    W(i)           =   (Vc(i)^2+Vn(i)^2)^0.5;       %Relative Velocity
    mub(i)      =  sin(angle(i))/(2+cos(angle(i)));
    Aoa(i)     =   (atan(mub(i)))*180/pi;
    Re(i)       =    0.019*W(i)/kv;
end
index=1;
Reynold_numbers= [x y z];
Real_angles = -30:30;
for i=1:180
    val = Re(i); %value to find
    tmp = abs(Reynold_numbers-val);
    tmp = sort(tmp);
    first_closest_RN = Reynold_numbers(1);
    second_closest_RN = Reynold_numbers(2);
    index_of_firstRN = find(A==first_closest_RN);
    index_of_secondRN = find(A==second_closest_RN);
    new(index,1) = val;
    for j=1:180
        val = Aoa(j); %value to find
        tmp = abs(Real_angles-val);
        tmp = sort(tmp);
        first_closest_AoA = Real_angles(1);
        second_closest_AoA = Real_angles(2);

        index_of_firstAoA1 = index_of_firstRN + first_closest_AoA + 31;
        index_of_secondAoA1 = index_of_firstRN + second_closest_AoA + 31;
        first_CL = A(index_of_firstAoA1,2);
        first_CD = A(index_of_firstAoA1,3);
        second_CL = A(index_of_secondAoA1,2);
        second_CD = A(index_of_secondAoA1,3);
        CL1 = (first_CL + second_CL)/2;
        CD1 = (first_CD + second_CD)/2;

        index_of_firstAoA2 = index_of_secondRN + first_closest_AoA + 31;
        index_of_secondAoA2 = index_of_secondRN + second_closest_AoA + 31;
        first_CL = A(index_of_firstAoA2,2);
        first_CD = A(index_of_firstAoA2,3);
```

```
        second_CL = A(index_of_secondAoA2,2);
        second_CD = A(index_of_secondAoA2,3);
        CL2 = (first_CL + second_CL)/2;
        CD2 = (first_CD + second_CD)/2;

        CL = (CL1 + CL2)/2;
        CD = (CD1 + CD2)/2;

        new(index+j,1) = val;
        new(index+j,2) = CL;
        new(index+j,3) = CD;
    end
    index = index+185;
end
```

3.3.3 Matlab Results:

Parameter	Value
The input/available power	10068.366960 [W]
The average Torque	-229.943840 [N.m]
The average Lift Force	1642.871677 [N]
The average Drag Force	627.308461 [N]
The average Thrust Force	-191.028161 [N]
The average Normal Force	1640.097306 [N]
The maximum value of Torque	2526.184360
The maximum value of Lift Force	3576.448205
The maximum value of Thrust force	1462.589370
The angular velocity of blades	198.959363 [RPM]
Head loss across turbine	0.017031 [m]
The power output of VAWT	-3877.013801
The Coefficient of Power of VAWT	-0.483032

Table 3.3

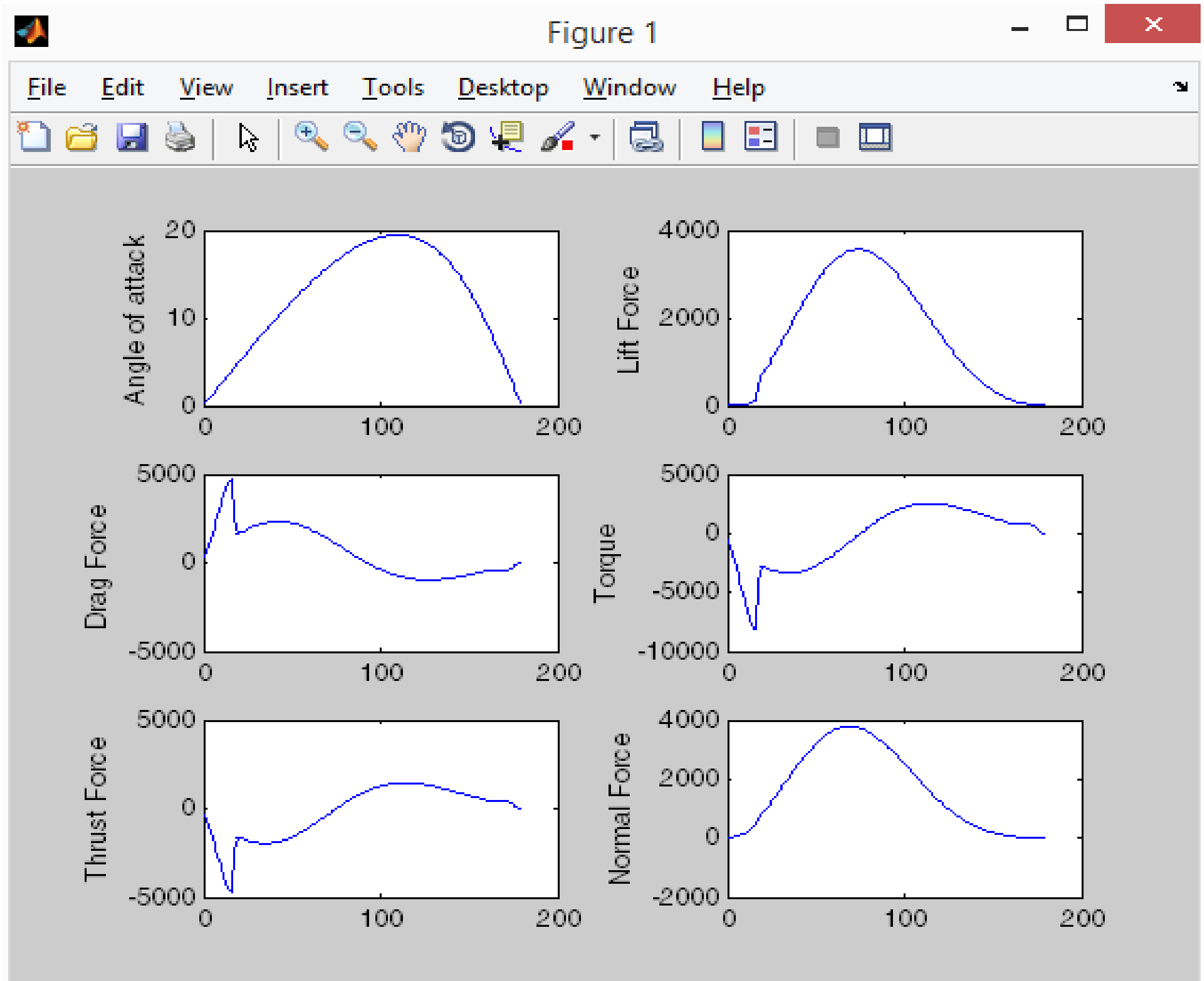

Figure 3.17 Matlab Results

After completion of theoretical calculations and simulations, the next phase was to test those results on an actual turbine. This objective was achieved by manufacturing a scaled down prototype of the turbine designed above. All the simulations run above were performed on the prototype as well and then they were tested against the actual performance of the prototype.

3.4 Prototype Designing:

The design process was the same as above, but, as the prototype is scaled down, all the related parameters have been scaled down accordingly as well.

The diameter of the pipe was taken to be 12 inches and so the diameter of the turbine will be 10 inches, so is the height.

3.4.1 Defining Parameters for Turbine Design:

1- Diameter of a pipe
2- Velocity of Water
3- Turbine Diameter
4- Turbine Height
5- Blade Air Foil
6- Solidity - Chord Length
7- Number of Blades

3.4.2 Blade Air Foil:

As mentioned earlier, NACA 4415 was selected for the original turbine since it gave better self-starting. This conclusion was reached not by mathematical or computational analysis but by experimentation. For simplicity's sake and ease of manufacturing, a symmetrical non cambered profile was selected for the prototype after having considered multiple symmetrical profiles. The one with the best Cl/Cd ratio was thus selected for the prototype.

The section 3.3 which covered the designing of original turbine was a consequence of the designing and testing of the prototype. And although it is mentioned earlier since it was the core objective of our project- to design a real time applicable turbine-it still is a result of the entire project of designing a prototype that we conducted.

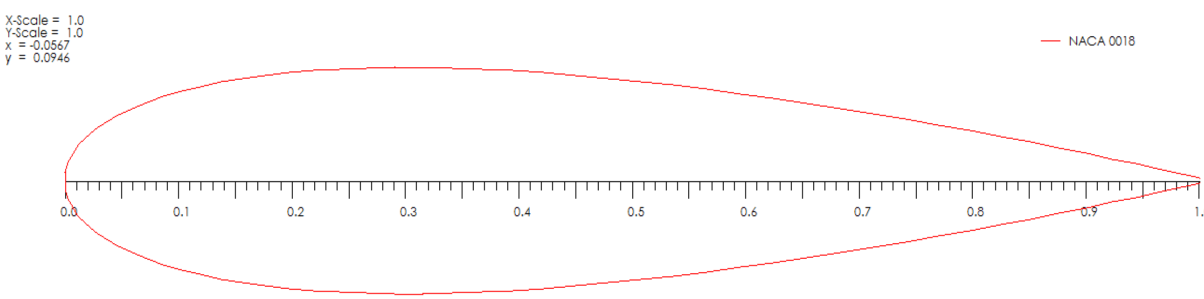

Figure 3.18 NACA 0018

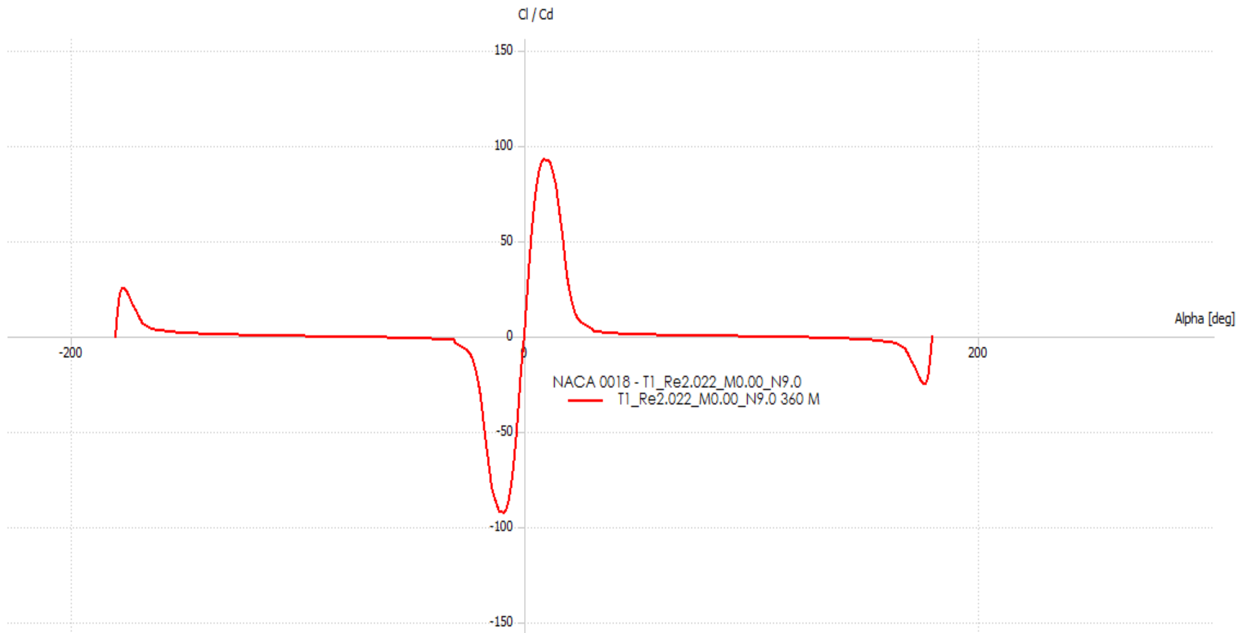

Figure 3.19 Cl/Cd vs α graph

3.4.3 Solidity - Chord Length:

As stated in the previous section, σ > 0.4 gave better self-starting. However, as can be seen from the table below, the chord length corresponding to solidity = 0.4 gives a chord length of 1.3 cm which is almost negligible for the profile to take proper visible shape. Since, the prototype was to be a working, but more importantly, a demonstrative model, it needed to be large enough to be able to present the blade profile in a proper manner, and so a solidity of 1.1 was selected with chord length = 3.5 cm.

Solidity	Chord
0.4	1.27
0.5	1.5875
0.6	1.905
0.7	2.2225
0.8	2.54
0.9	2.8575
1	3.175
1.1	3.4925
1.2	3.81
1.3	4.1275

Table 3.4

3.4.4 No. of Blades:

Except for the deliberate change in chord length, deviating from the ideal and optimum design condition, the rest of the parameters were kept constant such as TSR = 3, and No. of Blades = 4 so as to ensure control experiment model was closest to the original design.

Design parameters were so finalized as stated in the table:

Symbol	Parameter	Value
Air foil	NACA Profile	NACA 0018
D_p	Diameter of Pipe	12 inches
D_t	Diameter of Turbine	10 inches
V	Fluid Velocity	0.6 m/s
H	Blade Height	10 inches
R	Blade Radius	5 inches
λ	TSR	3.0
σ	Solidity	1.1
N	Number of Blade	4
C	Chord Length	3.5 cm

Table 3.5

3.4.5 A view of the Turbine profile input parameters:

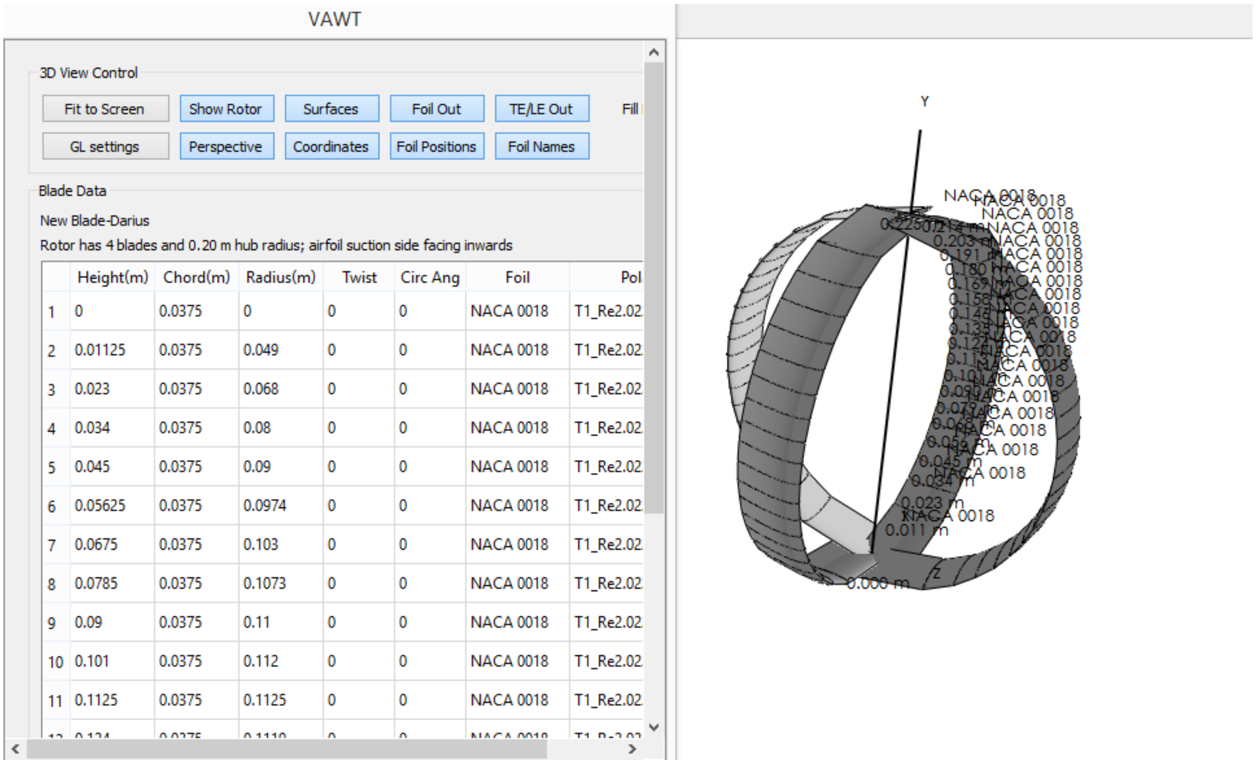

Figure 3.20 A view of the Turbine profile input parameters

3.4.6 Power vs TSR:

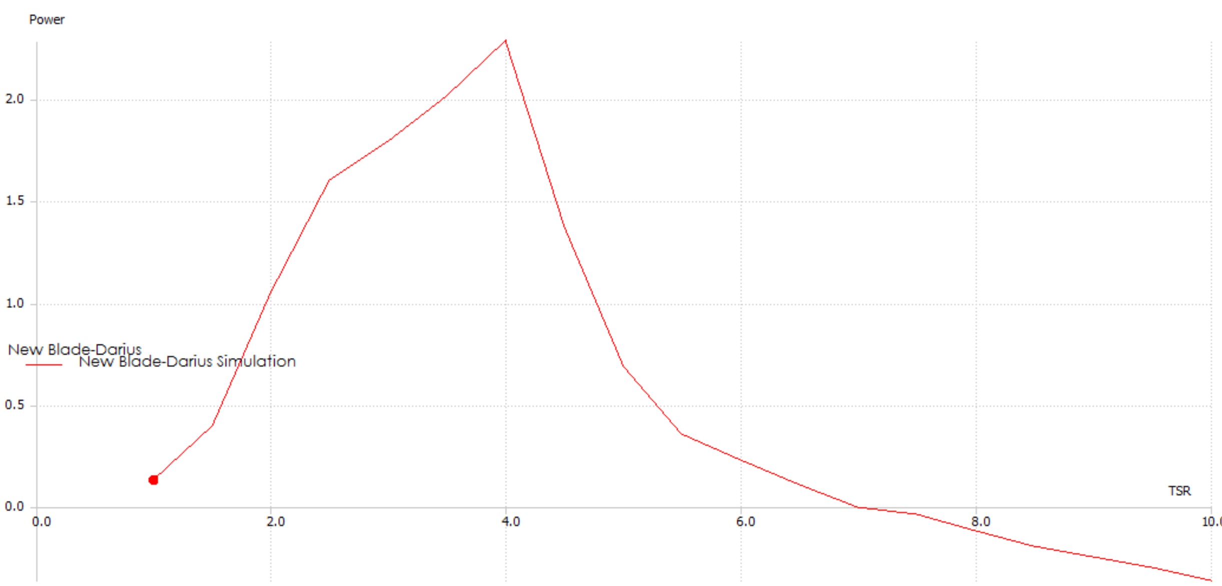

Figure 3.21 Power vs TSR graph

3.4.7 Torque vs TSR:

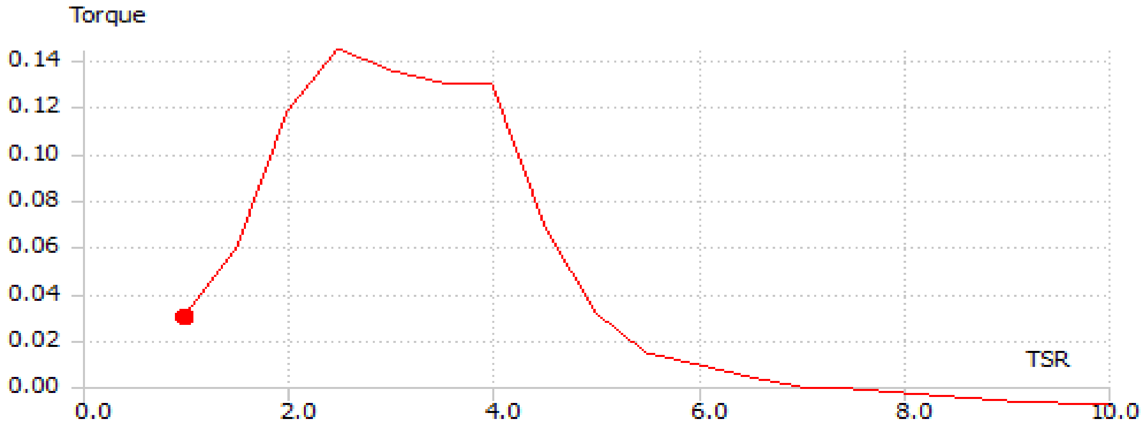

Figure 3.22 Torque vs TSR graph

3.5 Solid Modelling and ANSYS Simulation:

After completing the simulations in QBlade, a 3D model was created which was then exported to ANSYS for fluid simulation:

3.5.1 3-D Model Designing:

Solid works – a 3D Modelling software- was used to design the prototype.

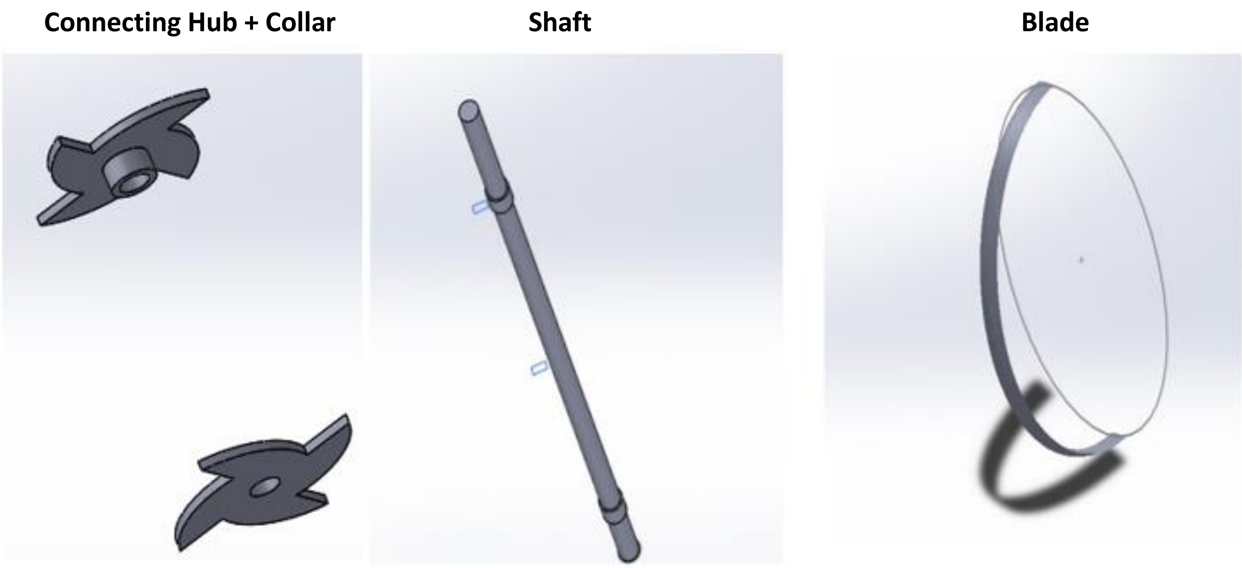

Figure 3.23 – Prototype parts

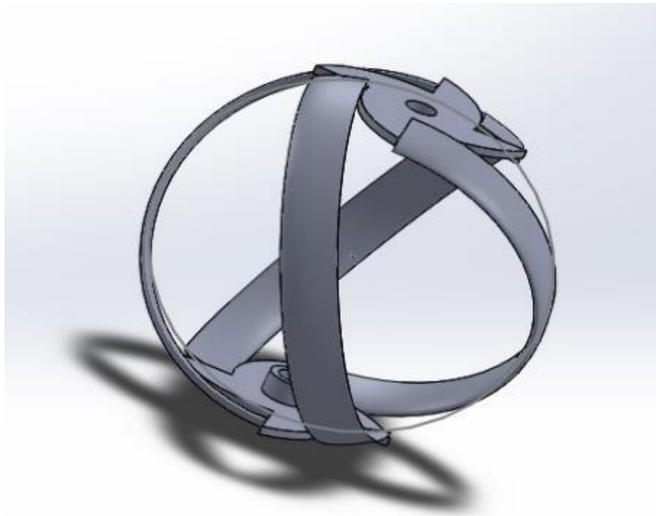

Figure 3.24 Turbine Assembly

3.5.2 Pipe Fitting:

The objective of our project was to design a power generation system that could be installed in water pipes. The model was thus fitted inside a pipe which was later imported to ANSYS for further analysis.

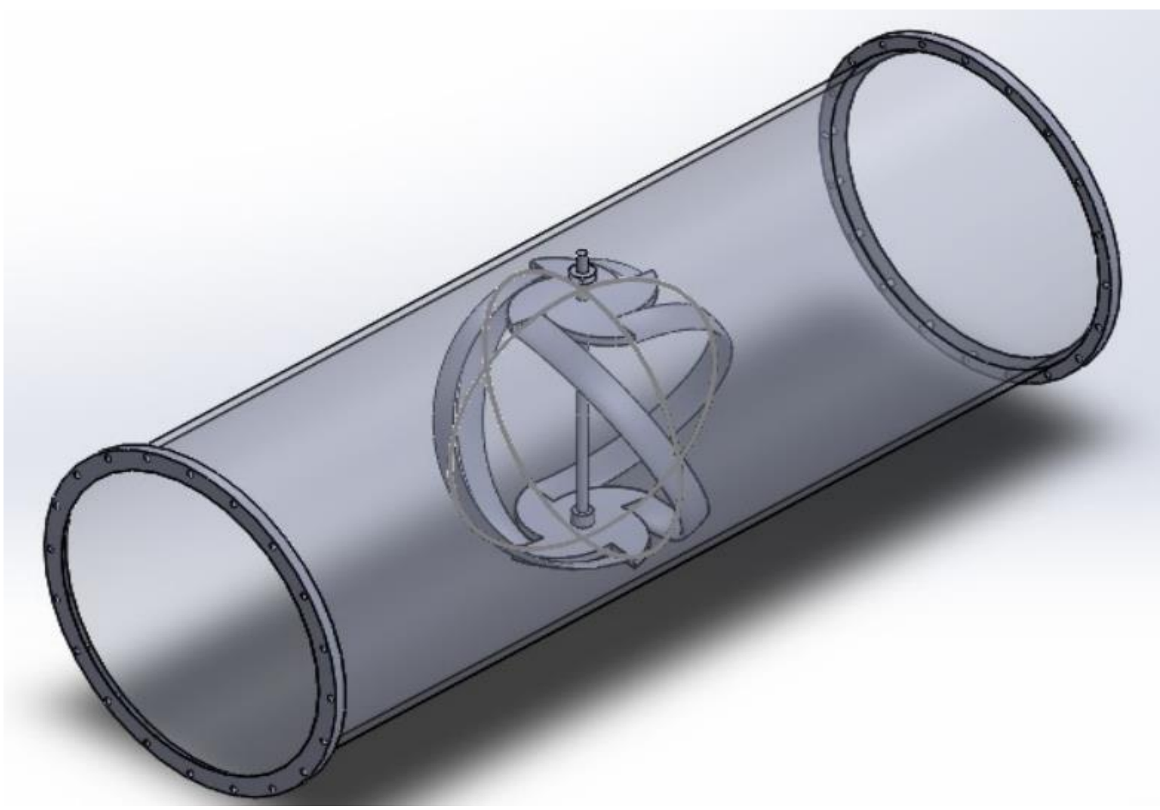

Figure 3.25 Turbine Assembly

3.6 ANSYS Simulation:

The model created was then exported to another simulation software, ANSYS where its interaction with the fluid was analyzed.

The main objective of a turbine design to extract energy from flowing fluid and convert it into electrical energy. The power output is calculated using the formula:

$$C_p = \frac{P}{\frac{1}{2}\rho A V_\infty^{\;3}}$$

The power coefficient Cp is a measure of conversion of water energy into actual electrical power output which effectively is the efficiency of a turbine. To determine the power coefficient, QBlade was used earlier. However, to verify and for further reassurance of the correctness of the results, a more complicated and thorough approach was pursued and ANSYS CFD Analysis of the turbine was done to find the Cp of the turbine.

3.6.1 CFD Analysis of the Turbine:

To analyze the complex and unsteady aerodynamic flow associated with hydro turbine functioning, computational fluid dynamics (CFD) is an attractive and powerful method. In this work, the influence of different numerical aspects on the accuracy of simulating a rotating hydro turbine is studied. In particular, the effects of mesh size and structure, time step and rotational velocity have been taken into account for simulation of different hydro turbine geometries.

At first, two-dimensional simulations are used in a preliminary setup of the numerical procedure and to compute approximated performance parameters, namely the torque, power, lift and drag coefficients. Then three-dimensional simulations are carried out with the aim of an accurate determination of the differences in the complex aerodynamic flow associated with the straight and the helical blade turbines. Static and dynamic results are then reported for different values of rotational speed.

3.6.2 Introduction:

The power coefficient of the turbine is estimated through two simulation methods in this study. First, a CFD simulation with the TSR given, similar to methods in other numerical studies, was used. Here, the rotational speed of the turbine axis is specified by user input. Second, a CFD simulation with a given load, that is called a flow-driven rotor simulation, is used. It is similar to an experimental approach, in which the rotational speed of the turbine axis is not fixed, but the turbine is rotated at a certain velocity upon the hydrodynamic moment on the blade, the inertia moment of the blade, and the given counter moment on the rotational axis. The instantaneous power generated by the turbine is equal to the product of the angular velocity (ω) of the turbine and the torque (T) acting on it. The power is not constant because the torque and velocity are not constant in the VAT. Hence, the average power per cycle is calculated as the product of the average values of these terms per cycle, as shown below

$$P = T\,\omega$$

The power coefficient (Cp) is then defined as

$$C_p = \frac{P}{\frac{1}{2}\rho A V_\infty^{\ 3}}$$

The numerical result is sensitive to the mesh quality in the boundary layer; hence, additional studies are necessary to check for numerical convergence before conducting further simulations.

3.6.3 Two-Dimensional Model and Results:

In this section, the geometrical features of the analyzed turbine are described first. Then, the adopted control volumes and the corresponding boundary conditions are described. The mesh generation parameters are also given.

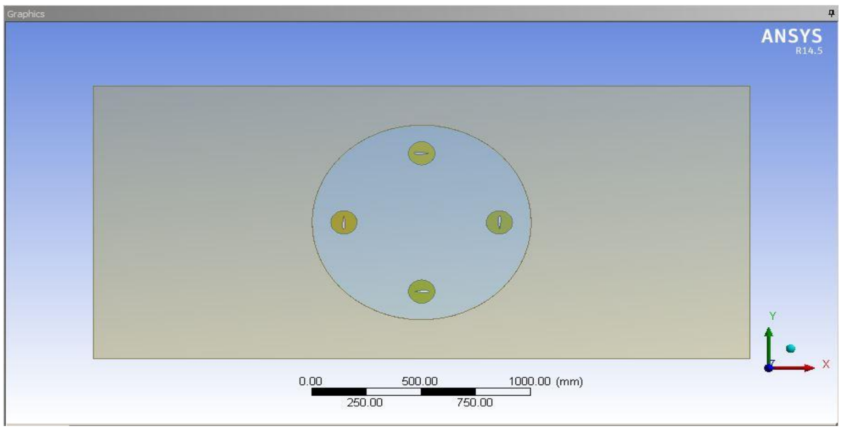

Figure 3.26

The solid geometry was created with a CAD modeler and imported into
a “Mesh Component Systems” in ANSYS® Workbench™, to create the mesh model.

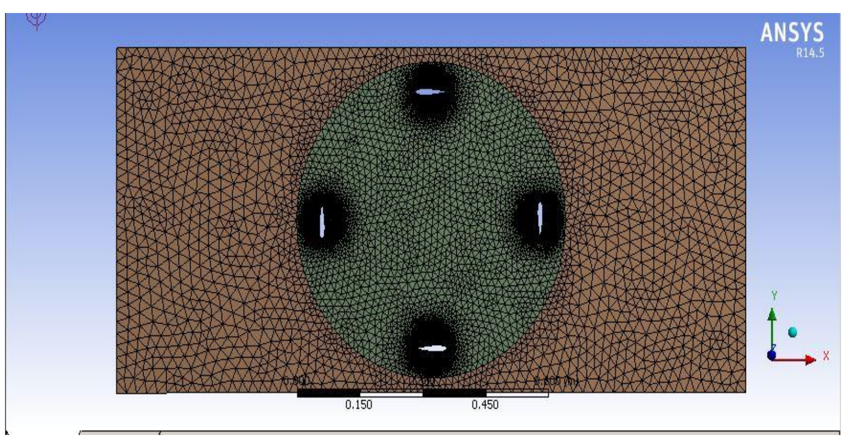

Figure 3.27

The discretized model generated was then read into FLUENTR for numerical solution. The geometric characteristics for the turbine are a NACA 0018 blade airfoil(chose from research study and Qblade® software results), with a chord length c = (different range through theoretical calculations) and a rotor radius R = 10 in.

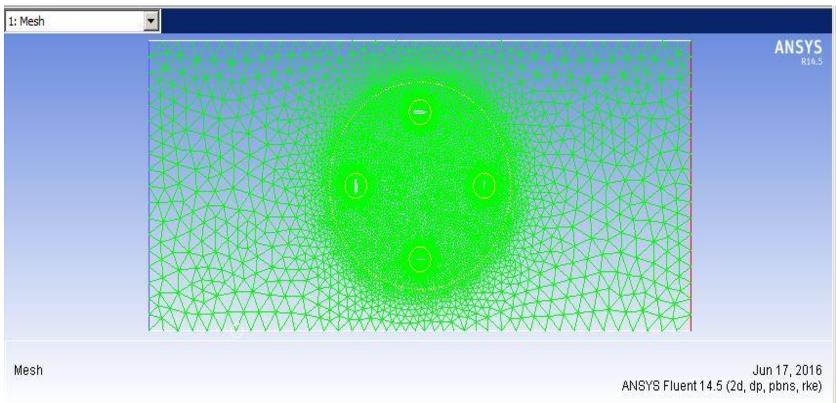

Figure 3.28

The length of the control volume along the free-stream direction is equal to Lx = 100R, while its width in the y direction is Ly = 60R.

The circular rotating domain has an overall diameter of Dr = 10 in.

At the velocity inlet, the velocity distribution is uniform, directed along the x-axis and equal to 3 m/s. The pressure outlet is set equal to 101,325 Pa. The no slip boundary condition is applied on the turbine wall blades. An interface wall is introduce between the fixed and rotating domain. The origin of the reference frame is the center of the rotor.

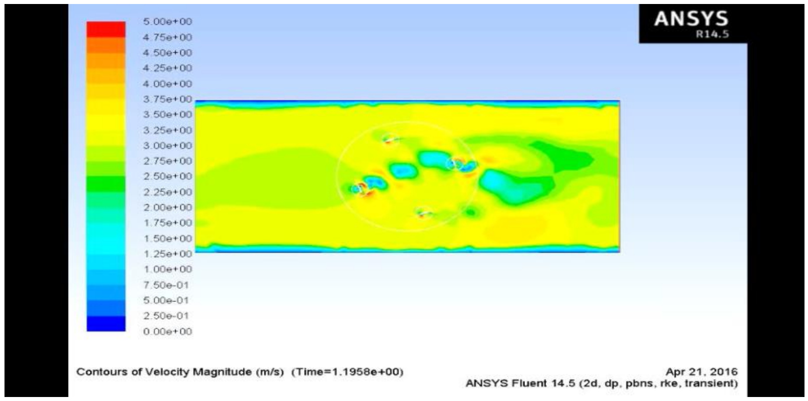

Figure 3.29

Now at different TSR λ value power co-efficient Cp was determined.

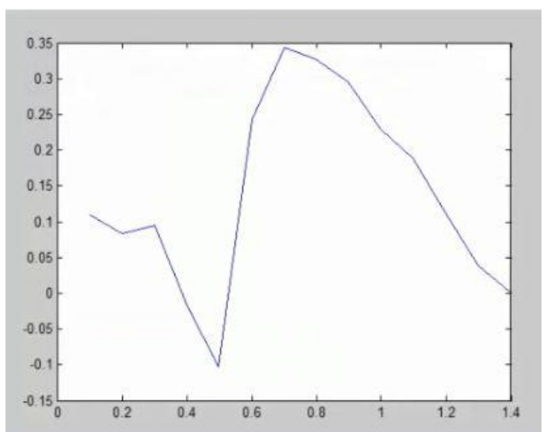

Figure 3.30 Cp vs TSR

3.6.4 Solver used:

K–omega (*k*–ω) turbulence model:

In computational fluid dynamics, the k–omega (*k*–ω) turbulence model is a common two-equation turbulence model, that is used as a closure for the Reynolds-averaged Navier–Stokes equations (RANS equations). The model attempts to predict turbulence by two partial differential equations for two variables, *k* and ω, with the first variable being the turbulence kinetic energy (*k*) while the second (ω) is the specific rate of dissipation (of the turbulence kinetic energy *k* into internal thermal energy).

Standard (Wilcox) *k*–ω turbulence model

The eddy viscosity ν_T, as needed in the RANS equations, is given by: $\nu_T = k/\omega$, while the evolution of *k* and ω is modelled as:

$$\frac{\partial(\rho k)}{\partial t} + \frac{\partial(\rho u_j k)}{\partial x_j} = P - \beta^* \rho \omega k + \frac{\partial}{\partial x_j}\left[\left(\mu + \sigma_k \frac{\rho k}{\omega}\right)\frac{\partial k}{\partial x_j}\right], \qquad \text{with } P = \tau_{ij}\frac{\partial u_i}{\partial x_j},$$
$$\frac{\partial(\rho \omega)}{\partial t} + \frac{\partial(\rho u_j \omega)}{\partial x_j} = \frac{\gamma\omega}{k}P - \beta\rho\omega^2 + \frac{\partial}{\partial x_j}\left[\left(\mu + \sigma_\omega \frac{\rho k}{\omega}\right)\frac{\partial \omega}{\partial x_j}\right] + \frac{\rho\sigma_d}{\omega}\frac{\partial k}{\partial x_j}\frac{\partial \omega}{\partial x_j}.$$

K-epsilon (k-ε) turbulence model:

K-epsilon (k-ε) turbulence model is the most common model used in Computational Fluid Dynamics (CFD) to simulate mean flow characteristics for turbulent flow conditions. It is a two equation model which gives a general description of turbulence by means of two transport equations (PDEs). The original impetus for the K-epsilon model was to improve the mixing-length model, as well as to find an alternative to algebraically prescribing turbulent length scales in moderate to high complexity flows.[1]

- The first transported variable determines the energy in the turbulence and is called turbulent kinetic energy (k).
- The second transported variable is the turbulent dissipation (ε) which determines the rate of dissipation of the turbulent kinetic energy

Standard k-ε turbulence model

The exact k-ε equations contain many unknown and unmeasurable terms. For a much more practical approach, the standard k-ε turbulence model (Launder and Spalding, 1974[3]) is used which is based on our best understanding of the relevant processes, thus minimizing unknowns and presenting a set of equations which can be applied to a large number of turbulent applications.

For turbulent kinetic energy k

$$\frac{\partial(\rho k)}{\partial t} + \frac{\partial(\rho k u_i)}{\partial x_i} = \frac{\partial}{\partial x_j}\left[\frac{\mu_t}{\sigma_k}\frac{\partial k}{\partial x_j}\right] + 2\mu_t E_{ij} E_{ij} - \rho\epsilon$$

For dissipation

$$\frac{\partial(\rho\epsilon)}{\partial t} + \frac{\partial(\rho\epsilon u_i)}{\partial x_i} = \frac{\partial}{\partial x_j}\left[\frac{\mu_t}{\sigma_\epsilon}\frac{\partial \epsilon}{\partial x_j}\right] + C_{1\epsilon}\frac{\epsilon}{k} 2\mu_t E_{ij} E_{ij} - C_{2\epsilon}\rho\frac{\epsilon^2}{k}$$

In other words,

Rate of change of k or ε + Transport of k or ε by convection = Transport of k or ε by diffusion + Rate of production of k or ε - Rate of destruction of k or ε

3.6.5 3D Solution:

Using the similar techniques 3d design was made using a CAD software with an inside rotating sphere to show the dynamic results of the turbine.

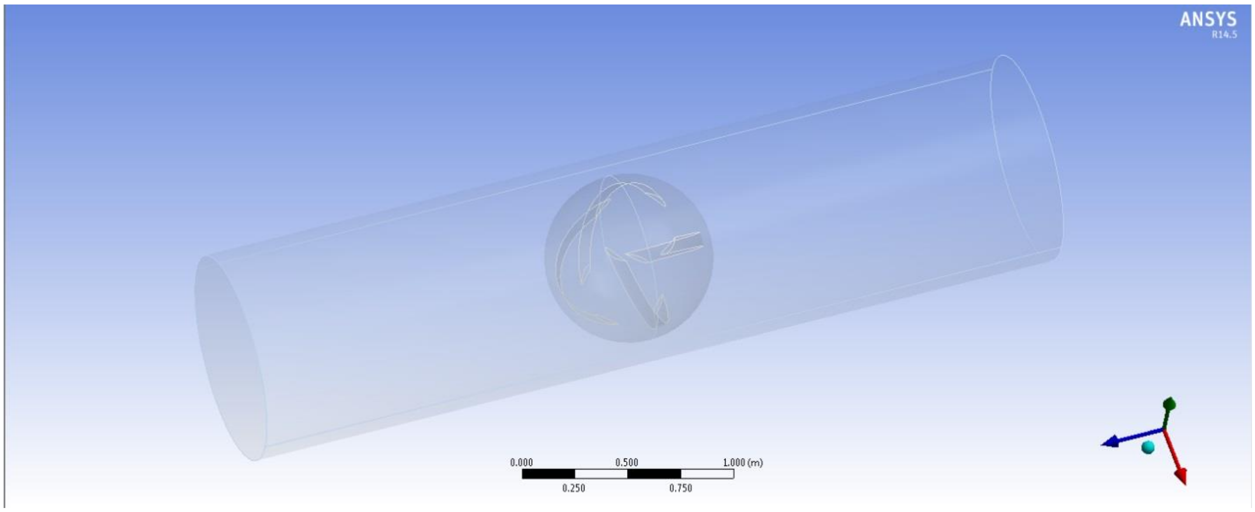

Figure 3.31 3D Solution

The mesh is characterized by tetrahedral elements. In particular, the maximum element size for the fixed domain is set to 0.5 m; the length of the element at the interface is equal to 0.05 m, whereas the minimum element size is 0.003 m and is used to discretize the fluid domain on the turbine wall.

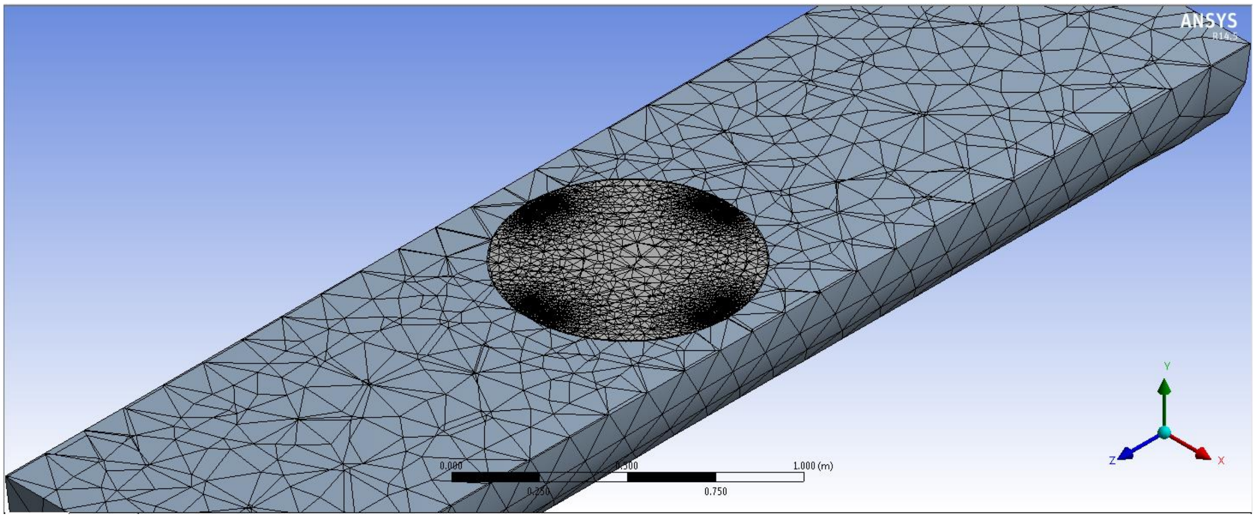

Figure 3.32 Mesh Result

After meshing the file was imported in Fluent and then using both k-ω and k-ε were used to find the results of the problem.

Velocity contour on blade:

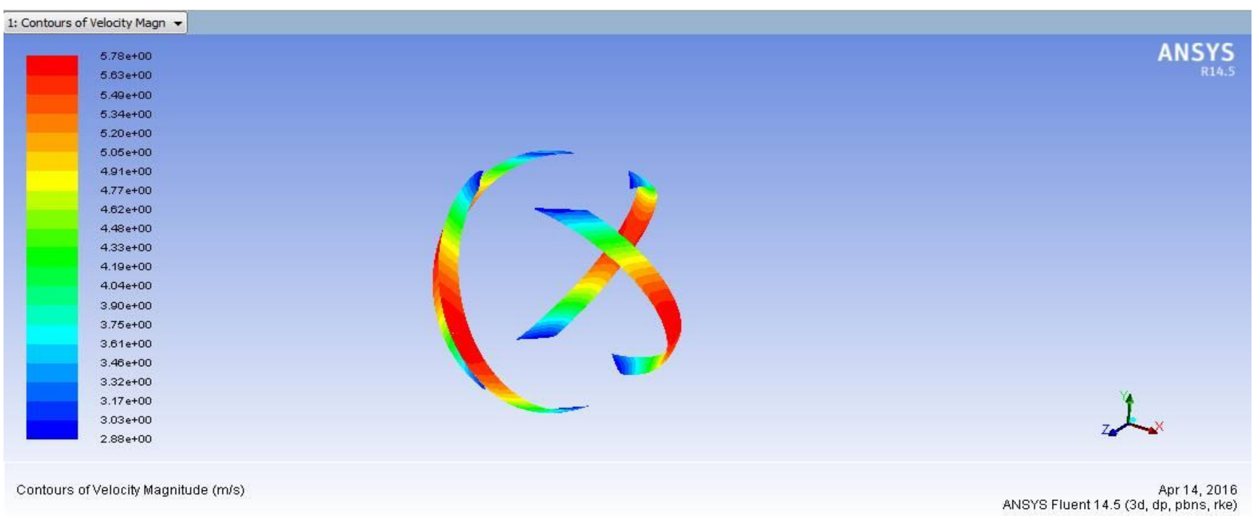

Figure 3.33 Mesh Result

Velocity Contour around the blade (rotating domain):

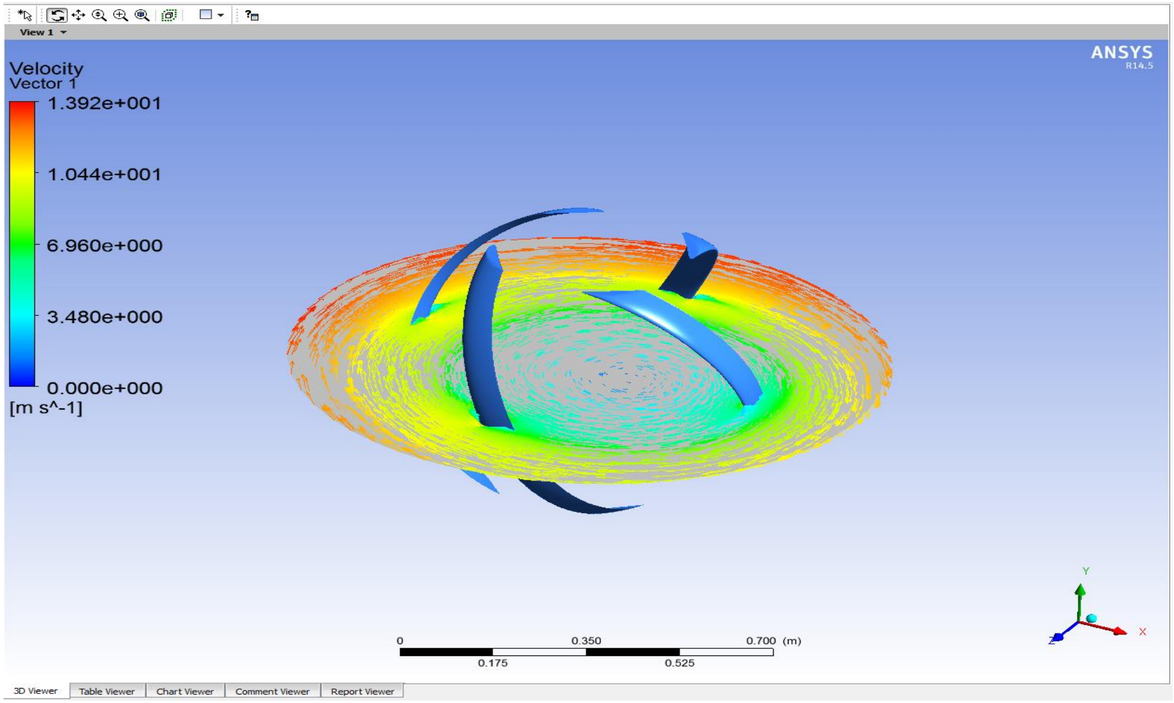

Figure 3.34

Pressure Contour around the blade:

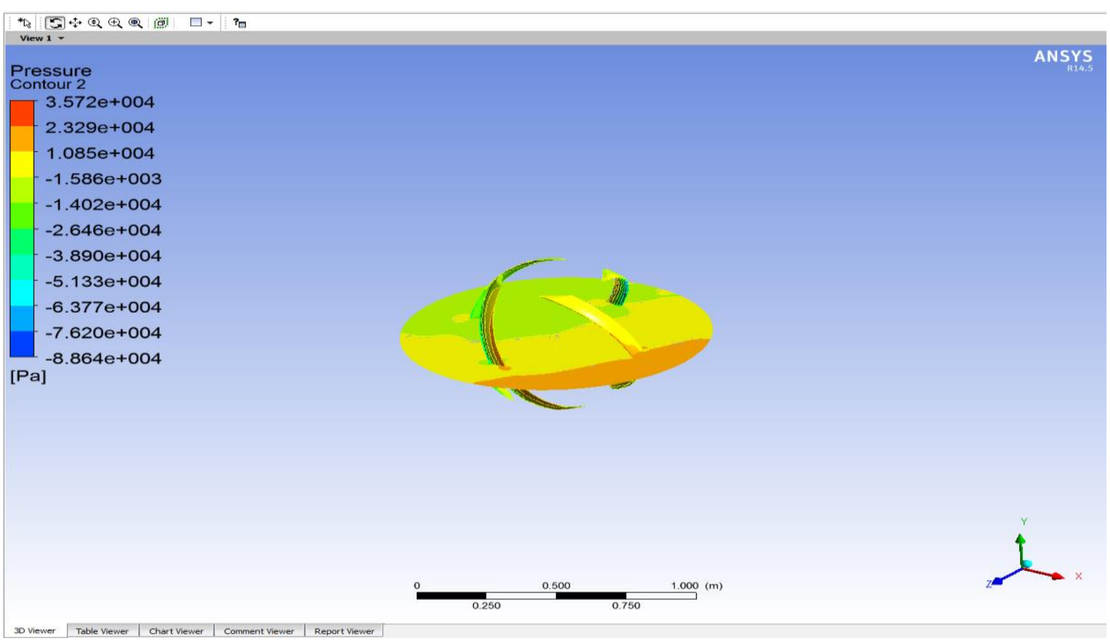

Figure 3.34 Mesh Result

3.6 Mathematical Results for Prototype:

The Matlab program was used to calculate the forces applied on the turbine as well as the power output of the turbine.

Parameter	Value
The input/available power	7.00 [W]
The average Torque	-19.450975 [N.m]
The average Lift Force	329.294077 [N]
The average Drag Force	125.736516 [N]
The average Thrust Force	-38.289322 [N]
The average Normal Force	328.737987 [N]
The maximum value of Torque	148.924586 [N.m]
The maximum value of Lift Force	716.856481 [N]
The maximum value of Thrust force	293.158634 [N]
The angular velocity of blades	90 [RPM]
Head loss across turbine	0.039995 [m]
The power output of VAWT	1.40 [W]
The Coefficient of Power of VAWT	0.2

Table 3.6

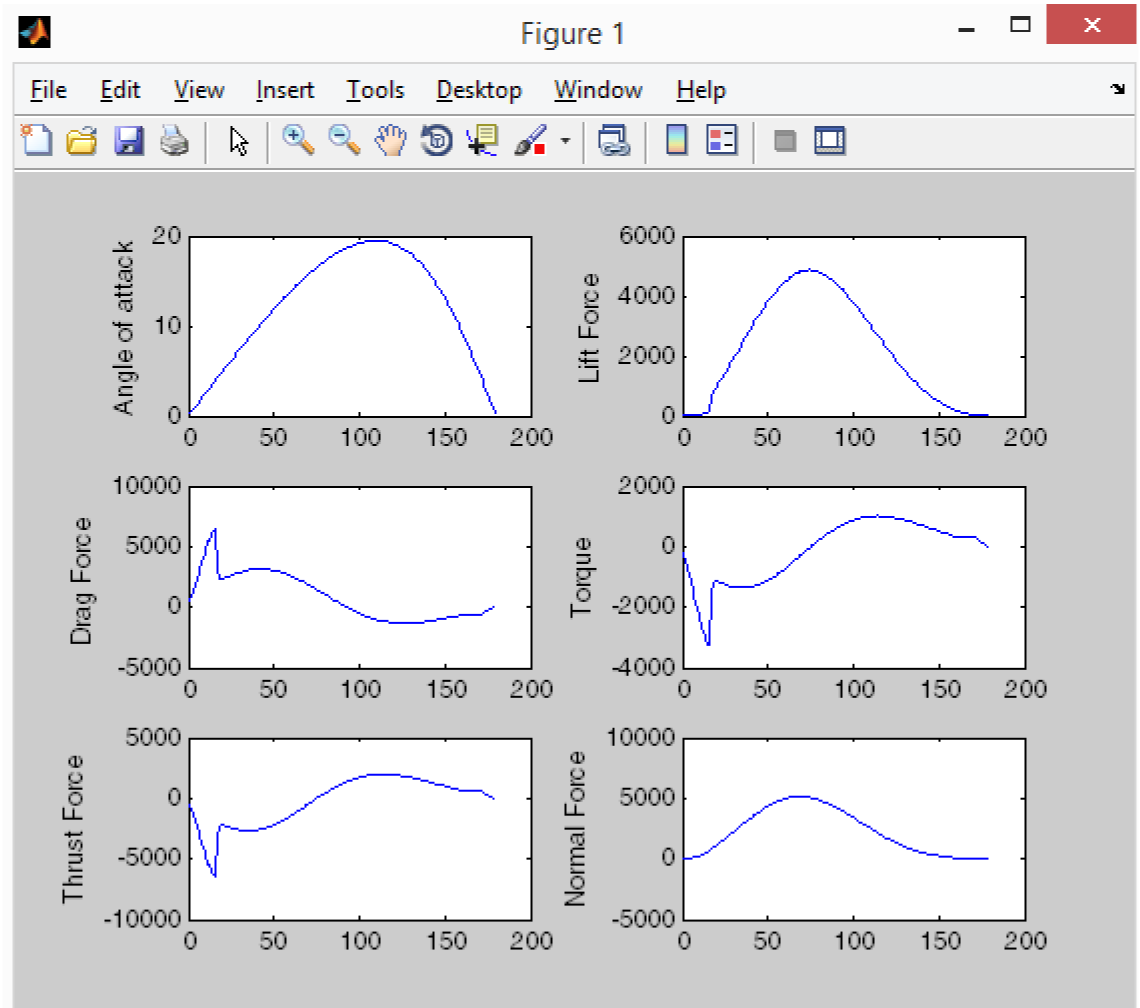

Figure 3.36 Matlab Results for Prototype

Chapter 4

Analysis (FEM)

FEM analysis was conducted on the prototype turbine and the results of simulation are mentioned below:

4.1 Structural Analysis:

Having completed fluid analysis on the turbine, the next step was to conduct material testing on the turbine. A structural analysis will provide the limits of operation of the turbine, in terms of rotational speed, in order to prevent structural failure. The forces calculated through Matlab program in **section 3.6** were used in the structural analysis of the turbine of the prototype.

4.1.1 Finite Element Analysis:

For our project, finite element analysis was performed in ABQUS as it being the most powerful FEA tool available.

4.1.2 Description of the Model:

Our model consists of 4 blades with each end attached to one upper and one lower hub. The upper and lower hubs are geometrical mirror of each other. In center, of the hub, a shaft is inserted to obtain mechanical power from the rotating turbine.

The model was designed in SOLIDWORKS and was imported in ABAQUS. All the parts were imported as independent entity.

4.1.3 Material:

For Shaft, following material properties were assigned to the cross section.
Density: 7800 [kg/m^3]
E: 193GPa
Poisson's ratio: 0.28

[ANSI Steel 316]

For the remaining parts, following material properties were assigned to the cross section

Density: 2700 [kg/m^3]

E: 69GPa

Poisson Ratio: 0.33

4.1.4 Assembly Module and Constraints:

After creating instances, all the parts were constrained accordingly.

In case of hubs, the partitioning was performed because of a bit complex geometry ABAQUS auto mesh was not able to mesh this part.

Steps:

After the built-in *initial* step, step one was created to apply loads on the blades

4.1.5 Load:

While considering the velocity of 0.6-1 [m/s], following loads were applied

1. Dynamic pressure load on all blades
2. Centrifugal load at 90RPM

4.1.6 Boundary Conditions:

Pin joint conditions were applied on the shaft ends.

4.1.7 Mesh:

As the model was partitioned previously, meshing was now an easy job. Due to the processing constraints, the seed size was kept at 20.

4.1.8 Results:

The obtained results were clearly in favor of the design prototype and no appreciable stresses were obtained in the results

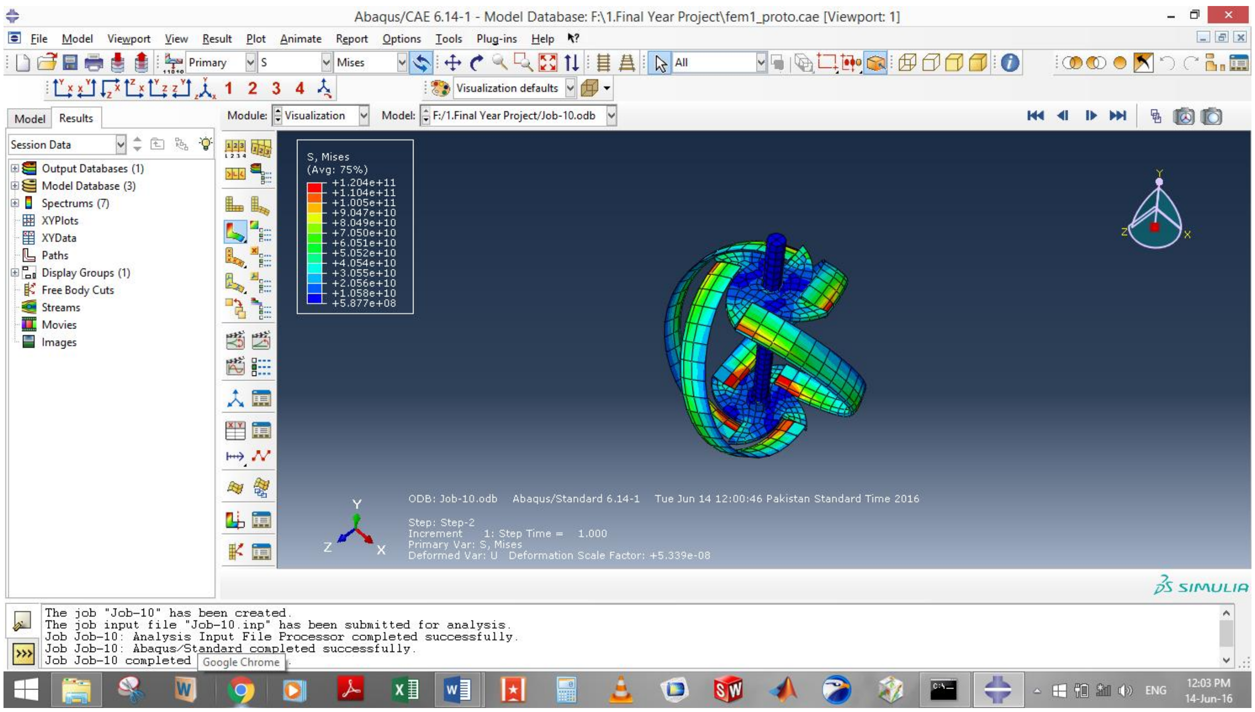

Figure 4.1

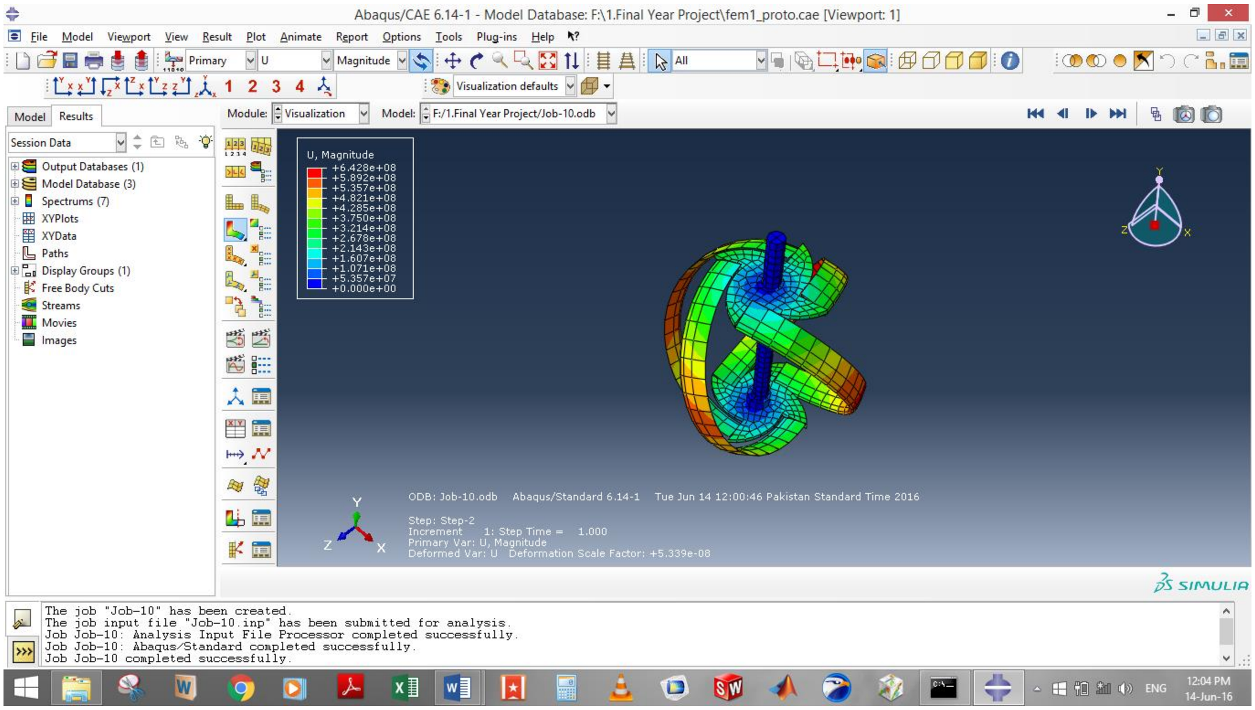

Figure 4.2

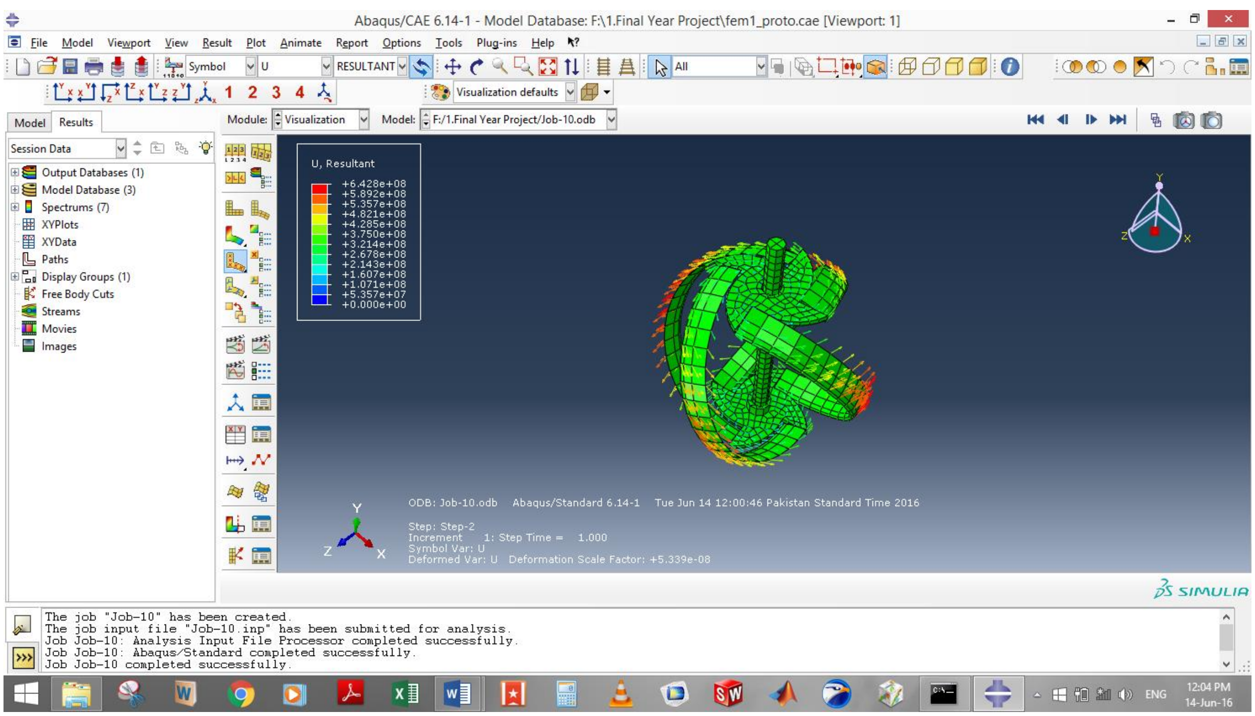

Figure 4.3

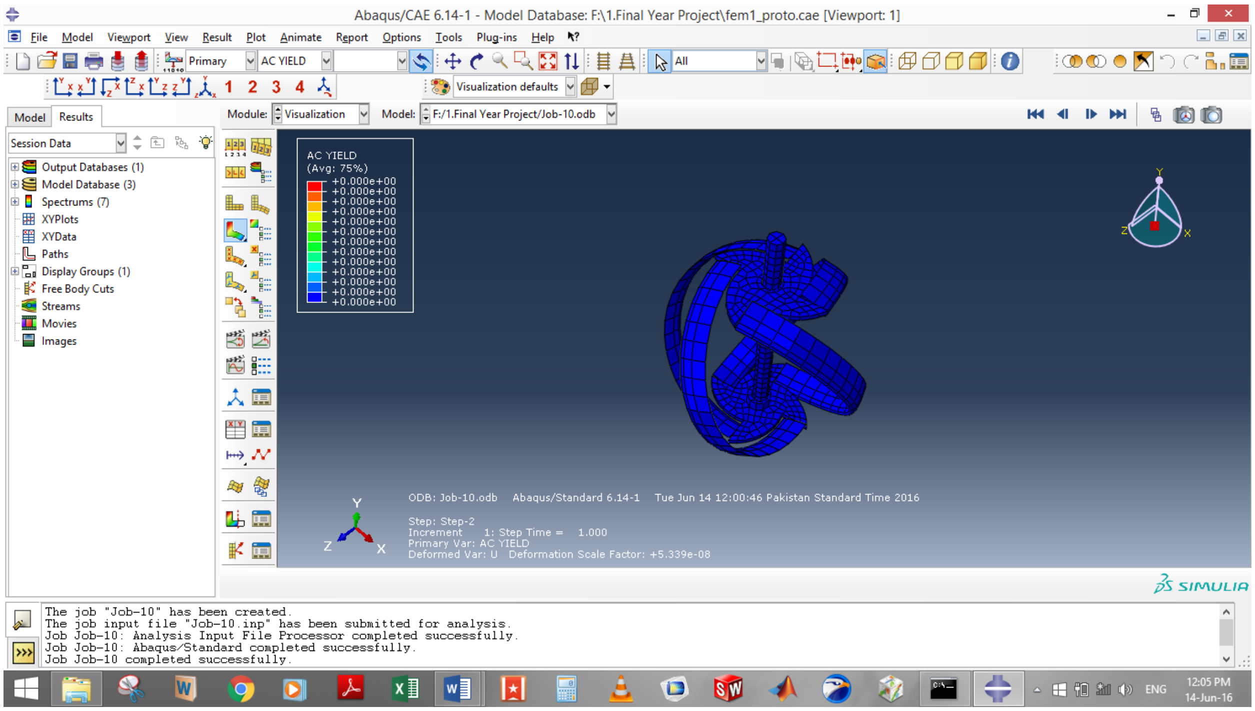

Figure 4.4

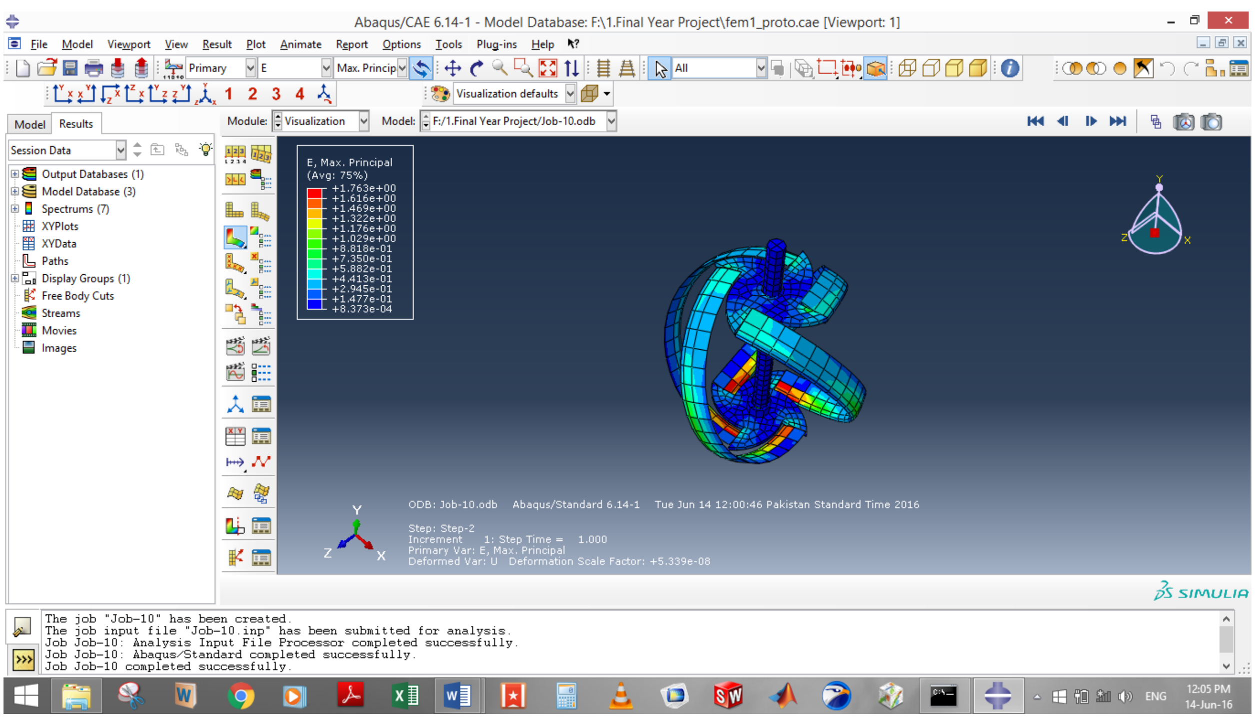

Figure 4.5

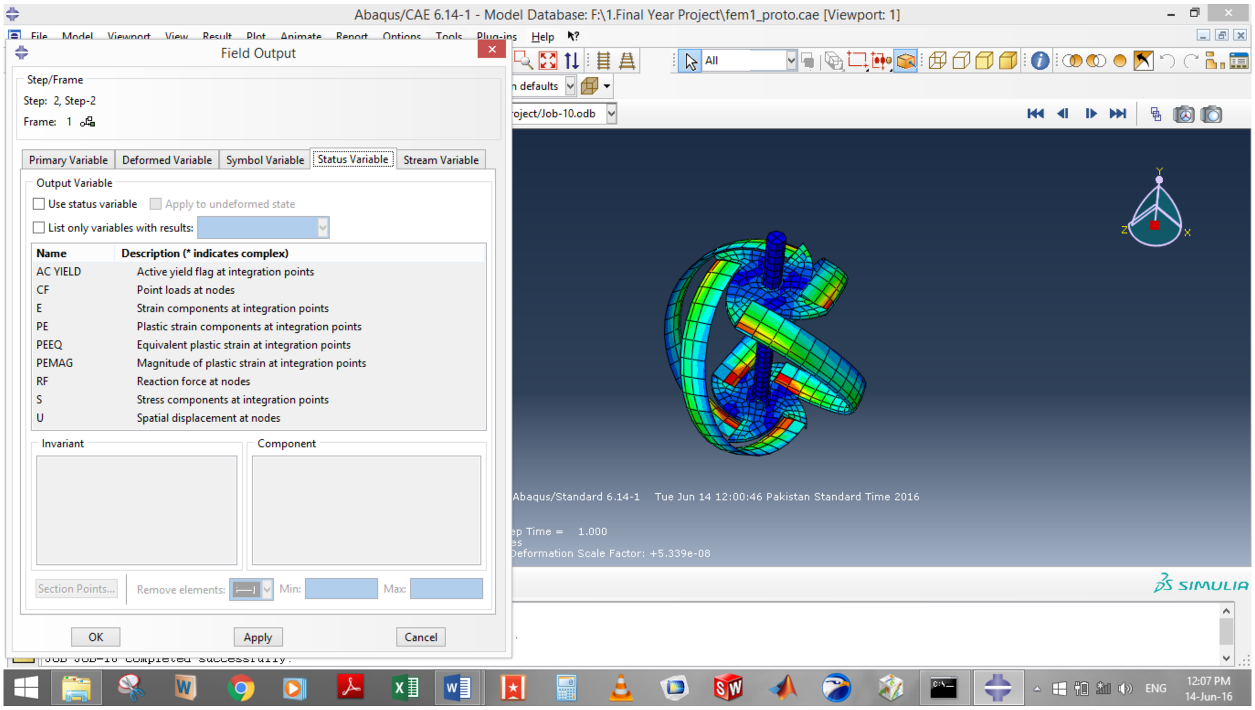

Figure 4.6

4.2 Fluid-Structure Interaction:

We tried our very best to do FSI analysis but were unable to create a proper interaction surface in the interaction module and therefore we are unable to present any results for that case.

4.3 Vibration Analysis:

The similar case happened in this case too. The natural frequencies results were so out of order and are unable to present.

4.4 Material Selection:

Material selection was done by the systematic approach set by Michael F. Ashby. Using systematic process defined by Ashby, we were able to narrow down materials from all material universe. In this process, however, we employed a software named CES EduPack which follows the same selection process defined by Ashby.

First, we applied some selection checks and limits in the software which narrowed down materials for us. After that, it was all just an engineering decision process.

This process can be understood by following images of the software interface. As basic principal, we decided the principal property to be Elastic Modulus as we want our blades to be in their original shape all the tame of their operational life as aerodynamic forces change rapidly with a slight variation in blade profile.

http://metalsupermarkets.com/blog/7-things-consider-choosing-aluminum-grade/

After careful study of various materials, it was eventually decided that Aluminum 6061 grade alloy was the most suited material for the turbine

Material Properties:

Grade Summary:

- This is the most versatile of the heat treatable aluminum alloys.
- This alloy offers a wide range of mechanical properties and corrosion resistance.
- It is easily fabricated and has good formability.
- It is weld-able using all methods including furnace brazing and so can retain properties with heat treatment.
- It has good machinability properties so buffing and other surface finishing processes can do done on it.
- It has medium to high strength for structural applications so can withstand constant force of water.

Chapter 5

Fabrication & Testing

5.1 Fabrication:

Aluminum was selected as the material for the casting of the turbine blades. Connecting hubs, collars as well the shaft were also made of aluminum which were all casted except for the shaft. The light weight and durable strength of the materials were major characteristics that were considered in choosing the material for the fabrication. Though these characteristics are exhibited by number of materials as well like composites but after considering the market availability, cost impacts and strength to wait ratio, we decided to use Aluminum for Micro Hydro turbine's manufacturing.

Following Manufacturing operations have been performed during turbine's manufacturing:

1. Turning
2. Drilling
3. Tapping
4. Dying
5. Drilling
6. Vertical Milling
7. Press fitting
8. Bench Fitting
9. Welding
10. Buffing

The turbine was fitted into a PVC pipe of 12'' inches.

The assembly was then taken to the site location for testing.

5.2 Prototype Testing:

Small canal near UET Taxila University was chosen for the testing of the prototype. The velocity at the location of testing was measured to be 0.6m/s.

For measurement of power output, a small DC motor was used as an alternator since the power output is considerably small, so using a motor was a reasonable choice. A small LED was also attached to show power generation as well as indicated in the figure.

MITSUMI

Stepping Motors

M42SP-13NK

FEATURES

1. High-output torque, and high resolution.
2. Superior running quietness and stability.

USES

Printers, multifunction machines, copy machines, FAX, etc

SPECIFICATIONS

Item	M42SP-13NK	
Rated Voltage	DC 12V	DC 24V
Working Voltage	DC 10.8~13.2V	DC 21.6~26.4V
Rated Current/Phase	600mA(PEAK)	
Coil DC Resistance	4.2Ω/phase±10%	
Step Angle	3.75°/step	
Drive Method	Constant Current	
Excitation Method	2-2 Phase excitation(Bipolar driving)	
Insulation Class	Class E insulation	
Holding Torque	56.9mN·m	56.9mN·m
Pull-out Torque	41.6mN·m/800pps	36.9mN·m/2,000pps
Pull-in Torque	46.6mN·m/200pps	46.6mN·m/200pps
Max. Pull-out Pulse Rate	1,800pps	3,900pps
Max. Pull-in Pulse Rate	880pps	880pps

CHARACTERISTICS

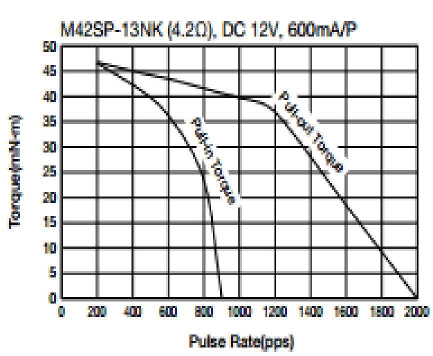

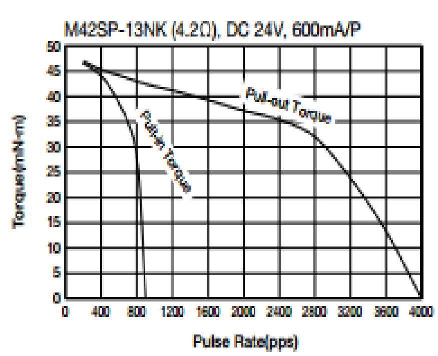

DIMENSIONS

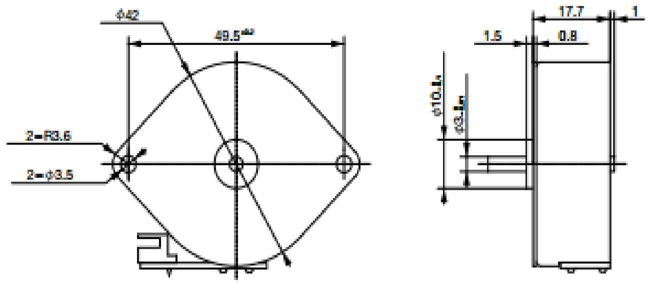

Unit : mm
General tolerance : ±0.5

- Any products mentioned in this catalog are subject to any modification in their appearance and others for improvements without prior notification.
- The details listed here are not a guarantee of the individual products at the time of ordering. When using the products, you will be asked to check their specifications.

Manual M42SP-13NK

Figure 5.1

Figure 5.2

Figure 5.3

Figure 5.4

5.2 Results:

The RPM measured was around 90 RPM.

The voltage measure was 2V as indicated in the figure of voltmeter above.

Since the motor is constant current motor of 0.6A,

Power output thus becomes P = V * I

P = 2 * 0.6

P = 1.2W

As discussed earlier, theoretical power output is calculated using the formula:

$$C_p = \frac{P}{\frac{1}{2}\rho A V_\infty{}^3}$$

Referring to table 3.6, Cp was found to be 0.2, putting in the equation above;

$P = ½*\rho * A * V^3 * C_p$

$P = 0.5 * 998 * 2 * (5*0.0254) * (10 * 0.0254) * 0.6^3 * 0.2$

P = 1.39W

% Difference = $\frac{1.39 - 1.2}{1.39} x\ 100$

= 14%

So a 14% difference in power output is seen between the theoretical and the actual results. The difference can be attributed to un refined casting of turbine blades and the efficiency of the motor which was used as an alternator.

The other major aspect of our core objectives was to create a system that has minimum head loss so that it creates least amount of problem for the transportation of water to its destination. Sufficient to say, **0.039995m head loss** calculated is much lower than we expected and thus, it fulfills our condition of designing such a system.

Although, the pressure drop could not be measure because of unavailability of pressure measuring device for a 12 inch diameter water pipe, power output validated by the practical tests give enough assurance to rely on the analytical results that they will coincide with the empirical ones.

Chapter 6

Conclusion and Recommendations

6.1 Conclusion:

- Aluminum 6061 is a suitable material for the turbine and is able to sustain the pressure applied by the water as validated by the stress analysis using Abacus as well.

- 4 Blade turbine is more efficient than 3 blade turbine and is better than 5 blade one in terms of pressure drop and economic consideration.

- There is an optimum rpm for turbine to work and that allows the system to achieve efficiency of 40 percent. However, results achieved were on lower water velocity and hence lower rpm, so Cp=0.2 was achieved. Imperfections in casted blades and motor efficiency also played their role in lowering the efficiency.

- Larger blades give much higher power output since power is directly proportional to square of its diameter. Also higher velocities increase the power manifolds since power is directly proportional to cube of water velocity.

- Experimental results though on the lower side but still are in very much agreement with the analytical results which makes it safe to assume that the original turbine calculations will prove to be accurate when applied to the piping system linking Simli Dam and the filtration plant ahead of it.

6.2 Recommendations:

Cambered profile was selected for the original turbine design with the intention of reducing starting torque application problem. That theory still needs to be tested in real time situation.

NACA profiles of only 4 digits were used. However, 5 or 6 digit profiles can be tested for research purposes since academic data is not in much abundance and it will give us new perspective as to possibilities attached with those profiles.

Helical angle allows for the rotation of the blades from any direction of water. However, the turbine was erected vertically and was tested in the same orientation in the canal. Testing it with varying orientations will also open new dimension of understanding the functioning of the turbine.

References:

Anderson, 2007. John D. Anderson. Fundamentals of Aerodynamics. ISBN: 007-125408-0. McGraw-Hill, 2007.

Blackwood, 2010. Marc Blackwood. Split Fin Physics. URL: http://www.scubaboard.com/forums/fins-masks-snorkels/325435-split-fin-physics.html, 2010. Accessed: 16-05-2011.

http://metalsupermarkets.com/blog/7-things-consider-choosing-aluminum-grade/researchgate.net/home

Int J Energy Environ Eng (2014) 5:333–340
DOI 10.1007/s40095-014-0129-x

mragheb.com/.../Vertical%20Axis%20Wind%20Turbines.pdf

Hydrodynamic Optimization
Method and Design Code for
Stall-Regulated Hydrokinetic
Turbine Rotors
D. Sale
University of Tennessee
J. Jonkman and W. Musial
National Renewable Energy Laboratory

Paraschivoiu, I. *Double-multiple streamtube model for Darrieus wind turbines*. 1981.